

# UC Irvine

## UC Irvine Electronic Theses and Dissertations

### Title

Nonlinear Optical Crosslinking (NLO CXL) of the Corneal Stroma

### Permalink

<https://escholarship.org/uc/item/9d6025k4>

### Author

Bradford, Samantha

### Publication Date

2019

Peer reviewed|Thesis/dissertation

UNIVERSITY OF CALIFORNIA,  
IRVINE

Nonlinear Optical Crosslinking (NLO CXL) of the Corneal Stroma

DISSERTATION

submitted in partial satisfaction of the requirements  
for the degree of

DOCTOR OF PHILOSOPHY

in Biomedical Engineering

by

Samantha Bradford

Dissertation Committee:  
Professor James V. Jester, Chair  
Professor Tibor Juhasz  
Professor Bernard Choi

2019

Chapter 1 © 2016 Journal of Cataract and Refractive Surgery

Chapter 2 © 2017 Biomedical Optics Express

Chapter 4 © 2018 Experimental Eye Research

All other materials © 2019 Samantha Bradford

# TABLE OF CONTENTS

	Page
LIST OF FIGURES	v
LIST OF TABLES	vii
ACKNOWLEDGMENTS	viii
CURRICULUM VITAE	ix
ABSTRACT	xi
INTRODUCTION	1
Keratoconus and Post LASIK Ectasia	1
Motivation	1
Crosslinking as a Treatment	2
UVA CXL	2
NLO CXL	5
CHAPTER 1: NLO CXL of Ex Vivo Rabbit Eyes	9
Introduction	9
Materials and Methods	10
Preparation of Eyes	10
Treatment of Eyes	11
Sectioning	12
Imaging and Quantification	13
SDS Page	13
Results	14
Discussion	17
CHAPTER 2: Custom Built NLO CXL Device	20
Introduction	20
Materials and Methods	20
Device Design	20
Effect of NA on Focal Volume	22
Preparation of Eyes	24
Treatment of Eyes	24
Mechanical Measurements	25
Sectioning and Imaging	27
Results	28
Control of Focal Volume and Depth	28
Change in Mechanical Stiffness	30

NLO CXL Induced CAF	32
Discussion	34
Issues	36
CHAPTER 3: Preliminary In Vivo Study	39
Introduction	39
Materials and Methods	39
Animals	39
In Vivo CMTF Imaging	40
Mechanical Testing	41
Results	42
CMTF	42
Discussion	44
CHAPTER 4: Collagen Fiber Crimping Analysis	45
Introduction	45
Materials and Methods	46
Animals	46
Treatment	47
In Vivo CMTF Imaging	48
CAF Imaging	48
Image Analysis	49
Results	51
CMTF	51
CAF	54
Collagen Crimping	55
Cellular Repopulation	57
Discussion	59
CHAPTER 5: Amplified NLO CXL	63
Introduction	63
Materials and Methods	64
Proof of Concept	64
Amplified Femtosecond Laser and Delivery	65
Stage 1: Supercontinuum Generation	67
Stage 2: Pump Formation	67
Stage 3: Parametric Conversion	67
Laser Delivery	68
Amplified NLO CXL in the Ex Vivo Rabbit Cornea	69
Scan Speed vs CAF	69
Corneal Stiffness Measurements	71
In Vivo Amplified NLO CXL	72
Results	73
Ex Vivo Amplified NLO CXL	73
Scan Speed vs CAF Intensity	73
Corneal Stiffness	75

In Vivo Amplified NLO CXL	76
Discussion	79
CHAPTER 6: Conclusions and Future Work	82
Conclusions	82
Crosslinking as a Treatment	82
Keratoconus and Post LASIK Ectasia	82
Myopia	82
Effects of Corneal Crosslinking	84
Future Work	84
Trans-epithelial Crosslinking	84
Further Investigation of Amplified NLO CXL	88
BIBLIOGRAPHY	89

## LIST OF FIGURES

		Page
Figure 1	Enhanced CAF after UVA CXL Treatment	3
Figure 2	Single vs. Multiphoton Excitation	7
Figure 3	Setup of NLO CXL	12
Figure 4	CAF Images of Corneal Sections	15
Figure 5	Average CAF Intensity of UVA vs. NLO CXL	16
Figure 6	SDS Page of Compressed Collagen Gel Treated with UVA or NLO CXL	17
Figure 7	Design of NLO CXL Delivery	21
Figure 8	NA vs Focal Spot Size	23
Figure 9	Design of Mechanical Indentation System	27
Figure 10	Images of Focal Volume	29
Figure 11	Beam Expander Setting vs Focal Volume	30
Figure 12	Force Required to Indent the Stroma	31
Figure 13	Corneal Elasticity after CXL	32
Figure 14	Corneal CAF after CXL	33
Figure 15	CAF Intensity after CXL	34
Figure 16	Stiffness of Acrylamide Gels	38
Figure 17	Example CMTF Image	41
Figure 18	CMTF Images of Initial In Vivo Study	43
Figure 19	CMTF Data of Initial In Vivo Study	43
Figure 20	Calculation of CFC	50

Figure 21	In Vivo CMTF Measurements	52
Figure 22	Cross Sectional CMTF Images	53
Figure 23	CAF after 1 and 3 Months	54
Figure 24	SHG Images of Collagen Crimping	56
Figure 25	Cellular Staining after Crosslinking	58
Figure 26	Single Spot Amplified NLO CXL	65
Figure 27	Custom NOPA Schematic	66
Figure 28	Amplified NLO CXL Induced CAF vs Speed	74
Figure 29	CAF Intensity vs Scanning Speed	75
Figure 30	Corneal Elasticity after Amplified NLO CXL	76
Figure 31	Short Term Amplified NLO CXL	77
Figure 32	Amplified NLO CXL Induced Corneal Flattening	78
Figure 33	Riboflavin Penetration across the Corneal Epithelium	87
Figure 34	Comparison of Trans-epithelial UVA and Amplified NLO CXL	88

## LIST OF TABLES

		Page
Table 1	Calculated Axial and Lateral Length, Focal Volume, and NA	29
Table 2	Corneal Thickness and Haze	53
Table 3	Collagen Fiber Crimp Data	56
Table 4	Scan Speed and Total Energy	70
Table 5	Corneal Flattening Data	79

## ACKNOWLEDGMENTS

There are a lot of people who deserve to be acknowledged for this project. Everyone from my family and friends, advisors, collaborators, lab mates and countless undergraduates played an instrumental role in the development of this dissertation. My Family and friends, especially my parents, have put up with me during this time and provided all the support I needed to finish a decade of schooling. I'm sure they're glad it's finally over.

My co-advisors Dr. Jester and Dr. Juhasz have proven invaluable troves of knowledge. Dr. Jester did his best to teach me a thing or two about biology while we tinkered with lasers, and was always there when directions were needed. Dr. Juhasz always knew where to find the answers to the hardest problems, and I'll always appreciate the lunch breaks that came with his visits. Dr. Brown was also always there to help with the project, even though he didn't have to. Whether it was helping with experiments or providing a distraction in the form of a story about Montana, it was greatly appreciated.

My lab mates were also indispensable in this work. Our post doc Eric Mikula spent hours hunched over the optical table to prepare for experiments, and was always willing to teach me all he knew. Dongyul Chai helped gather the preliminary data that started this project and taught me how to build the dreaded poker. Yilu Xie was always willing to help me stain samples even when she didn't have the time. She knows where everything in the lab is hidden; we'd all be lost without her. Dr. Kim spent hours teaching us how to use an Orbiscan, when no one else could. I'd also like to mention the countless undergraduates who have helped me throughout the years. They work willingly and happily and make the lab run smoothly. They do everything from dishes to countless hours of data processing. They're traced hundreds of collagen fibers, and dripped countless eyes. Without them this dissertation would have taken at least twice as long.

Also, the following grants are gratefully acknowledged: NIH grant EY24600, Skirball Program in Molecular Ophthalmology, Research to Prevent Blindness, Inc. (RPB 203478), and KFS PR14728 (445043-19954)

# CURRICULUM VITAE

## Samantha Bradford

- 2013            B.S. in Biological Engineering, University of Missouri, Columbia
- 2014-19        Graduate Student Researcher, Department of Ophthalmology, University of California, Irvine
- 2016            M.S. in Biomedical Engineering, University of California, Irvine
- 2016-19        Teaching Assistant, Department of Biomedical Engineering, University of California, Irvine
- 2019            Ph.D. in Biomedical Engineering, University of California, Irvine

## PUBLICATIONS

Bradford, S.M., Brown, D.J., Juhasz, T., Mikula, E., Jester, J.V., 2016. Nonlinear optical corneal collagen crosslinking of ex vivo rabbit eyes. *Journal of cataract and refractive surgery* 42, 1660-1665.

Bradford, S.M., Mikula, E.R., Chai, D., Brown, D.J., Juhasz, T., Jester, J.V., 2017. Custom built nonlinear optical crosslinking (NLO CXL) device capable of producing mechanical stiffening in ex vivo rabbit corneas. *Biomed Opt Express* 8, 4788-4797.

Bradford, S.M., Mikula, E.R., Juhasz, T., Brown, D.J., Jester, J.V., 2018. Collagen crimping following in vivo UVA-induced corneal crosslinking. *Experimental eye research* 177, 173-180.

## CONFERENCES

Association for Research in Vision and Ophthalmology (ARVO) Conference, May 2015. Poster Presentation: Rapid, Single Pass, Highly focused Nonlinear Optical Collagen Crosslinking (NLO CXL) of Ex Vivo Eyes.

Association for Research in Vision and Ophthalmology (ARVO) Conference, May 2016. Paper Talk: Corneal Crosslinking and Mechanical Stiffening Using Nonlinear Magic.

Association for Research in Vision and Ophthalmology (ARVO) Conference, May 2017.  
Paper Talk: Collagen Fiber Crimping Following in vivo UVA-induced Corneal  
Crosslinking.

Gordon Research Seminar, Cornea and Ocular Surface and Pathology, February 2018.  
Poster Presentation: Precise Trans-epithelial Nonlinear Optical Crosslinking (NLO CXL)  
Using Amplified Femtosecond Pulses.

Gordon Research Conference, Cornea and Ocular Surface and Pathology, February  
2018. Poster Presentation: Precise Trans-epithelial Nonlinear Optical Crosslinking (NLO  
CXL) Using Amplified Femtosecond Pulses.

# **ABSTRACT**

Nonlinear Optical Crosslinking (NLO CXL) of the Corneal Stroma

By

Samantha Bradford

Doctor of Philosophy in Biomedical Engineering

University of California, Irvine, 2019

Professor James V. Jester, Chair

Ectatic disorders of the cornea such as Keratoconus or post-LASIK ectasia are characterized by mechanical weakening and thinning of the corneal stroma, leading to distortion of its shape and severely impacting the vision of those affected. Though temporary vision correction can be achieved, advanced cases often require corneal transplants. A new method, recently approved by the FDA, has the potential to stop or reverse the progression of disease. For this procedure the cornea is presoaked in the photosensitizer riboflavin and irradiated with ultraviolet-A (UVA) light. The riboflavin then generates oxygen free radicals, causing covalent bonds to form between corneal collagen molecules, mechanically stiffening the tissue. In order to avoid the potential cellular damage associated with UVA irradiation specific parameters have been selected for this procedure which minimize exposure to deeper structures, especially to the corneal endothelium which is not regenerative in humans. Unfortunately these parameters limit crosslinking (CXL) to the anterior cornea and allow for very little control over the treated area.

We have hypothesized that the substitution of nonlinear excitation for UVA irradiation would greatly increase the precision of this procedure, thereby improving its safety and efficacy. We have termed this technique nonlinear optical crosslinking or 'NLO CXL.' NLO CXL uses highly focused 760 nm femtosecond laser light to induce two photon excitation of the riboflavin soaked within the corneal tissue, limiting photo activation to the focal volume, and allowing for highly controllable crosslinking in the x, y, and z directions. Also, near infrared light is generally not harmful to cellular structures and naturally penetrates much deeper into corneal tissue than UVA light. Because of this the focal volume can be positioned much deeper into the tissue without taking the risk of damaging the endothelium.

This body of work details, first and foremost, the development of a system that is capable of producing a nonlinearly crosslinked volume of corneal collagen, with highly controllable dimensions. It also presents the results of studies intended to develop a better crosslinking procedure overall, including general exploration of the effects of crosslinking on corneal collagen or shape.

# Introduction

## Keratoconus and Post LASIK Ectasia

The collagen matrix which makes up the corneal stroma provides strength and shape to the cornea, allowing it to properly focus light to the retina in the back of the eye. When the mechanical properties of this matrix are altered, so is the eye's overall refractive power. In the case of corneal ectatic diseases such as Keratoconus or post LASIK ectasia, this collagen matrix is weakened. This weakening leads to corneal thinning, a cone-shaped protrusion, and declining visual acuity. Keratoconus, specifically, is a non-inflammatory disease characterized by progressive biomechanical weakening of the cornea.<sup>1, 2</sup> It affects 1 out of every 2000 people in the general population<sup>3</sup> and is the leading cause for corneal transplantation surgery.<sup>4</sup> Post LASIK ectasia is a very similar condition which results as a complication of refractive surgery. It is currently estimated to affect 1 out of every 4500 patients.<sup>5</sup>

## Motivation

It is thought that mechanically strengthening the weakened tissue by inducing crosslinking of the collagen fibers using the irradiation of ultraviolet A (UVA) light, a technique introduced by Spoerl and Wollensak<sup>6, 7</sup> and recently approved by the FDA, can prevent the need for surgery by slowing, or reversing progression of disease. Current attempts at UVA crosslinking (UVA CXL) of corneal collagen have been successful for Keratoconus patients, but lack control over the precise region of crosslinking, possibly exposing more tissue than necessary to harmful irradiation. This report explores a more

precise method of corneal crosslinking, termed nonlinear optical crosslinking (NLO CXL), which has the potential to increase the safety and efficacy of corneal collagen crosslinking.

## **Crosslinking as a Treatment**

### *UVA CXL:*

The standard UVA CXL protocol (Dresden Protocol), as described by Spoerl and Wollensak,<sup>6-8</sup> requires that the corneal epithelium be removed in order to soak the stroma with a photosensitizing riboflavin solution (0.1% in PBS, 20% high fraction dextran). The solution is dripped onto the surface every 2 minutes for 30 minutes to allow for full riboflavin penetration of the stroma. It is then irradiated with 370 nm UVA light at an irradiance of 3 mW/cm<sup>2</sup>, with 5.4 mJ, for 30 minutes. This wavelength of light activates the riboflavin molecules which causes the production of oxygen free radicals which then induce covalent crosslinks between and within the collagen fibers.<sup>8, 9</sup> Conveniently, induced crosslinking has also been proven to enhance blue collagen auto fluorescence (CAF).<sup>10</sup> By exciting corneal sections with 760 nm light and collecting 400-450 nm light, the treated region can be imaged as shown in Figure 1.

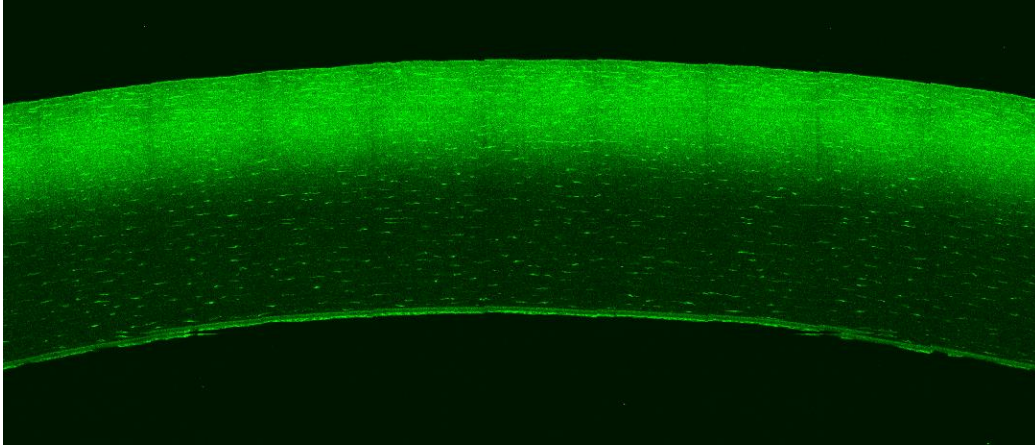


**Figure 1: Enhanced CAF after UVA CXL Treatment**

Example of enhanced CAF between 400-450 nm in a cornea treated with UVA CXL, Dresden protocol.

This treatment, which has been tested clinically and approved by the FDA, shows an increase in the stiffness of human corneas up to 300%, and a 2-3 fold increase in corneal elastic modulus.<sup>7, 11</sup> Research thus far suggests that this method is capable of delaying the progression of ectatic disease and improving visual acuity. Furthermore, recent clinical studies indicate that crosslinking not only halts the progression of corneal disease, but is also capable of corneal flattening by an average of one diopter after six months of treatment, lasting at least 24 months.<sup>7, 12-19</sup> This opens the possibility for broadening the range of the procedure to include the treatment of low refractive errors. While this procedure has demonstrated many desirable effects, it is not without disadvantages.<sup>14, 20, 21</sup>

This treatment has many known effects on corneal tissue, including a dose dependent cellular toxicity, corneal haze, and collagen fiber thickening up to 12% within the crosslinked region.<sup>7, 12, 14-16, 22</sup> In particular, keratocytes and endothelial cells are both at risk of damage, as cell death occurs within the crosslinked volume.<sup>22-26</sup> It has previously been observed that keratocyte repopulation begins around one month post crosslinking

in rabbits, but reports in the literature of full cellular repopulation vary widely. Wollensak reported full cellular activity by 6 weeks,<sup>25</sup> but others reported a continuing presence of acellular areas and apoptotic changes such as apoptotic bodies, shrunken cell nuclei, and chromatin condensation, especially around the periphery of irradiation.<sup>23, 24, 27</sup> Keratocyte damage is inevitable with this procedure, but endothelial cell damage is a greater concern. It has been found that UVA irradiance higher than 0.36 mW/cm<sup>2</sup> is enough to damage the non-regenerative human endothelial cell layer.<sup>22</sup> The parameters of standard UVA CXL were carefully chosen to reduce these risks, and the risk of corneal endothelial damage is only reached in corneas thinner than 400 µm.<sup>28</sup> This means that patients who have progressed further into their disease are not eligible for standard treatment.

Another weakness of this technique is its overall lack of precision. Some degree of control over the lateral position of crosslinking could be accomplished by applying a mask to the surface of the cornea, but this is both potentially uncomfortable for the patient and heavily dependent on the surgeon's judgement. Also the volume of crosslinking begins at the corneal surface, going only as deep as UVA light can penetrate into the tissue, diminishing in effectiveness with depth.<sup>8</sup> This means that any attempt to perform trans-epithelial UVA CXL, however successful in the stroma, would still damage the epithelium in the process.

Many of these weaknesses are due to the nature of the single photon excitation process being utilized. Single photon excitation occurs when one photon of a specific wavelength is used to excite a molecule to a higher energy level. In the case of UVA CXL, one photon of UVA light holds enough energy to excite a molecule of riboflavin to the

excited singlet state. If the excited singlet riboflavin undergoes intersystem crossing to an excited triplet state then a free oxygen radical can be produced. The free radical then induces covalent crosslinking of collagen fibrils. Without intersystem crossing the excited riboflavin returns to the ground state energy level via green fluorescence.<sup>9</sup> Because the excitation occurs so easily, UVA light will excite all of the riboflavin in the optical path, quickly leading to attenuation as a function of depth reducing the efficiency of crosslinking deeper within the cornea (Figure 2). Prolonged riboflavin excitation also leads to photo-bleaching and loss of riboflavin excitation and collagen crosslinking. Also oxygen concentration within the cornea has been shown to be depleted within 15 seconds of the onset of standard UVA CXL treatment, returning to normal 3 to 4 minutes after crosslinking. This depletion is much more dramatic in accelerated UVA CXL (which uses a higher irradiance of 30 mW/cm<sup>2</sup> for a shorter time) occurring within 5 seconds, and has thus hampered the ability to significantly shorten crosslinking time for individual patients.<sup>9</sup> To reduce the risk of damage, and improve the efficacy of crosslinking treatments there is a great need to control the area of crosslinking both laterally and axially.

### *NLO CXL:*

Many of the concerns of UVA CXL can be addressed by changing the manner of riboflavin activation to a nonlinear, multiphoton, process. Previous studies have already shown that collagen hydrogels can be mechanically stiffened via crosslinking using a nonlinear optical approach.<sup>29</sup> In contrast to the single photon excitation of UVA CXL, two photon, or nonlinear excitation, of riboflavin uses a longer wavelength, lower energy light to excite riboflavin within a defined optical volume. Two photon excitation occurs when

two photons of half the original excitation energy simultaneously (within  $10^{-15}$  s) excite the same molecule. This event occurs within an area of exceptionally high photon density, such as that created by focusing high intensity, very short pulsed femtosecond (fs) laser light. By the nature of this reaction, oxygen free radicals are only produced in the small volume of photo activated riboflavin within the focal region. The focal volume can then be scanned throughout the cornea to treat a much larger volume, allowing for very localized and depth controlled crosslinking, and mechanical stiffening of the cornea to a similar degree achievable by UVA CXL in a much more precise manner. Also near infrared light is much safer to cells than UVA light, minimizing the risk of collateral cellular damage outside the focal volume.

Figure 2 demonstrates the increased precision of multiphoton activation by comparing images of the fluorescence within two tanks of riboflavin solution. The image in 2A shows two photon excitation using focused 760 nm fs laser light. The excited area is limited to the focus of the beam which can be moved to any depth within the sample. In contrast, the image in 2B demonstrates single photon excitation using a 370 nm light source. In this image photo activation is seen only at the surface.

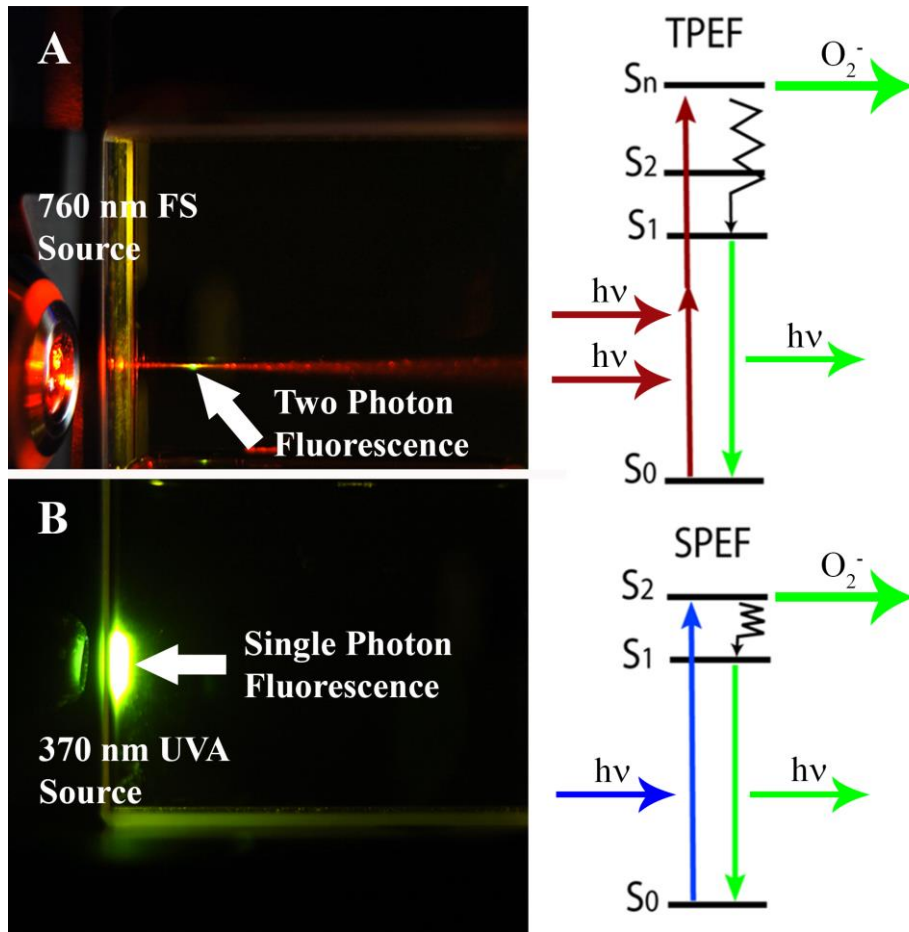


**Figure 2: Single vs. Multiphoton Excitation**

(A) Two photon excitation of riboflavin solution using a 760 nm fs laser and the Jablonski diagram demonstrating two photon excitation. (B) Single photon excitation of riboflavin solution using a 370 nm light source and the associated Jablonski diagram.

The substitution of nonlinear excitation for UVA irradiation has many benefits over single photon excitation. Near infrared light has a much higher transmission through the cornea, and therefore a greater depth of penetration than UVA light, eliminating attenuation of the light at deeper stromal depths. Furthermore, since riboflavin can only be activated in the focal volume there is no photo-bleaching of the riboflavin above or below the region being crosslinked. Also, there is no generation of free radicals outside the region of crosslinking leading to greatly reduced oxidative cellular damage. Finally,

limiting photoactivation to the focal volume allows for highly controllable crosslinking in x, y, and z directions, and therefore precise regional stiffening within the cornea using patterns that can be designed based on individual patient topographies.

It is likely that NLO CXL follows the same principles as traditional UVA CXL with regards to oxygen dependency since it is still dependent on riboflavin excitation. However, the small excitation volume and shortened excitation time using NLO CXL might limit oxygen depletion in the surrounding tissue. Specifically, for all of the experiments contained in this report, NLO CXL only excites a very small focal volume of tissue, from 182.8-1407.1 femtoliters (Table 1), for no more than 1.6 ms (far less when amplified pulses are utilized), possibly limiting oxygen depletion and/or allowing sufficient oxygen diffusion from the surrounding tissue.

Another important note pertaining to the differences between the two methods of crosslinking is the potential of NLO CXL to effectively perform trans-epithelial crosslinking. This is of particular clinical interest since epithelial debridement is a painful portion of the procedure. While both techniques are hampered by the ability to perfuse enough riboflavin past an intact epithelium, only NLO CXL will have the ability to leave the epithelium undamaged once this is accomplished. As previously stated, UVA CXL must begin at the surface of the tissue, while NLO CXL can be performed at any depth, avoiding unwanted exposure within the intact epithelium.

# Chapter 1: NLO CXL of Ex Vivo Rabbit eyes

## Introduction

In previous studies it has been shown that compressed type I collagen hydrogels can be mechanically stiffened to a degree similar to that achieved by UVA CXL by using the NLO CXL technique described to photoactivate riboflavin in defined regions.<sup>29</sup> While Chai et al.<sup>29</sup> demonstrated this technique's ability to produce localized and depth controlled crosslinking and mechanical stiffening of collagen hydrogels, its highly focused laser light required multiple passes at different depths to achieve a large crosslinked volume. This required a time commitment of multiple hours limiting its clinical practicality. Addressing these concerns was the first main goal of this project, and was accomplished by adjusting the scanning parameters, mainly focal size and scanning speed, to optimize the approach. Theoretically, a lower numerical aperture (NA) objective should expand the two photon focal volume.<sup>30</sup> With the correct speed a larger focal volume could ideally produce similar results to those reported by Chai et al.<sup>29</sup> in a much shorter time. The purpose of these initial experiments was to determine whether NLO CXL could be achieved, and its optimal parameters, in intact ex vivo rabbit eyes using a low NA lens for rapid, single pass, enlarged focal volume CXL.<sup>31</sup> The experiments in this chapter served as a proof of concept prior to the development of a custom device.<sup>32</sup>

## Materials and Methods

### *Preparation of eyes:*

Seventeen whole globe, ex vivo rabbit eyes were included in this study. They were shipped to the laboratory fresh (Pel-Freez, Rogers, AR), rinsed in minimal essential medium (Invitrogen, Carlsbad, CA) and placed in a 12 well tissue culture plate filled with the same medium to just below the corneal/ scleral limbus. They were then incubated in a 5% CO<sub>2</sub> humidified incubator at 37°C for at least one hour prior to further preparation. After incubation a small spot was tattooed at the limbus of each eye to serve as a fiducial marker during treatment, and an 8 mm diameter area of the epithelium was scraped from the center of each cornea using a Tooke knife.

Eyes were segregated into four groups. Control 1 eyes (2) were left completely alone, epithelium intact, no soaking, and no treatment. Control 2 eyes (2) underwent epithelial removal and were soaked in 0.5% riboflavin-5-phosphate solution (Sigma-Aldrich, St. Louis, MO) in phosphate-buffered saline (PBS; pH 7.2) with 20% high-fraction dextran, molecular weight of 450-650 KDa, (Sigma-Aldrich, St. Louis, MO) by dripping the solution onto the corneas every 2 minutes for 30 minutes, but were not irradiated in any way. Control 3 eyes (2) were soaked in the same manner in 0.1% riboflavin solution with 20% dextran and placed under a 370 nm UVA lamp, with continued dripping throughout the treatment. The fourth group consisted of eleven eyes soaked in 0.5% riboflavin, 20% dextran solution and treated with expanded focal volume NLO CXL at various effective scan speeds. A higher concentration of riboflavin was used for this group because it has been suggested that this can offset lower dwell times.<sup>30, 33</sup>

### *Treatment of eyes:*

Prepared eyes were held inside of a glass coverslip bottom Petri dish (MetTek, Corporation, Ashland, MA) and mounted over the objective of a Zeiss LSM 510 confocal microscope (Carl Zeiss, Jena, Germany) as shown in Figure 3. The fiducial marker was placed to the far right during scanning to put it in line with the scan lines. Using a 4x, 0.1 NA Zeiss Apochromat objective (Carl Zeiss) a theoretical excitation volume, calculated to be 150  $\mu\text{m}$  axial and 3  $\mu\text{m}$  lateral using the equations outlined by Zipfel et al.,<sup>30</sup> was generated with 1W of 760 nm fs, 80 MHz, laser light (Chameleon, Coherent Inc., Santa Clara, CA). Corneas were then raster scanned with 4  $\mu\text{m}$  line separation at pixel dwell times varying from 204  $\mu\text{s}$  to 1.63 ms over a 4.5 by 2.25 mm area in the central anterior cornea. Specifically, this was accomplished by adjusting the imaging parameters within the microscope's software. 512 by 512 lines were scanned in each of two tiles, 2 by 1, for each sample, producing the desired 4  $\mu\text{m}$  line spacing. Then a combination of the number of times a line was repeated (line averaging) and the dwell time of each pixel was adjusted to produce a desired range of total pixel dwell times. For the sake of clarity, the total pixel dwell time was converted to a measure of the effective speed of scanning. For example, an eye treated with a dwell time of 204  $\mu\text{s}$ , and line averaging of eight would have a total pixel dwell time of 1.63 ms, and a corresponding scanning speed of 2.69 mm/s.

After 30 minutes of soaking in the described riboflavin solution, UVA CXL control eyes were irradiated with 370 nm UVA light at 3 mW/cm<sup>2</sup>, 5.4 mJ, for 30 minutes with continued dropping of riboflavin solution as described by Spoerl et al.<sup>28</sup> After treatment the corneas were excised and fixed overnight in 2% paraformaldehyde (PFA, Mallinckrodit Baker, Inc., Phillipsburg, NJ) in PBS at 4°C.

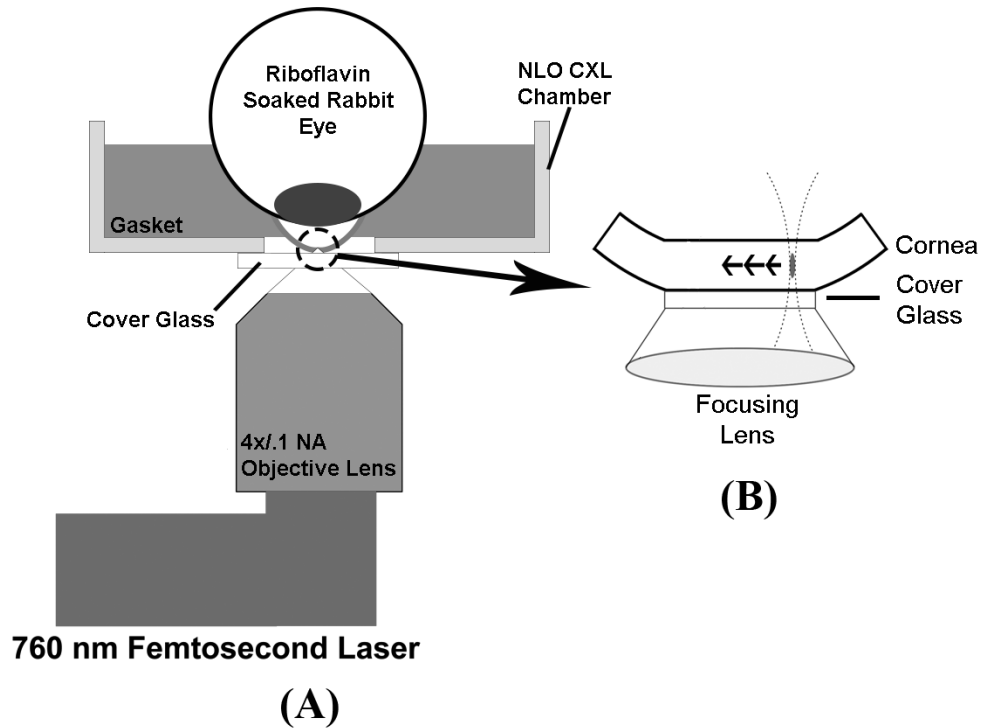


**Figure 3: Setup of NLO CXL**

(A) Prepared eyes were positioned above the 4x/ 0.1 NA objective of a Zeiss LSM 510 confocal microscope. (B) A spot was generated using 760 nm fs laser light focused approximately 150  $\mu\text{m}$  into the corneal tissue. The spot was then raster scanned over two tiles, totaling a 2.25 by 4.5 mm area. Reprinted/ adapted with permission from the Journal of Cataract and Refractive Surgery.<sup>31</sup>

### *Sectioning:*

After fixation, corneas were sectioned to prepare for imaging. The bottom third of each cornea was cut away, perpendicular to the marker, and therefore perpendicular to the line of crosslinking, and embedded straight edge down in 10% low melting point agarose (Lonza, Rockland, ME). The samples were then sectioned to a thickness of 250  $\mu\text{m}$  using a vibratome (Campden Instruments, Loughborough, England). Each slice was floated off and stored in 2% PFA in PBS at 4°C until ready for imaging.

### *Imaging and Quantification:*

Sections closest to the center of the cornea were then examined for CAF, which is indicative of collagen crosslinking, as demonstrated previously.<sup>10, 27, 31, 32</sup> Sections were scanned with the Zeiss LSM 510 confocal microscope using two photon excitation at 760 nm with a 40X oil immersion objective (1.3 NA). Emissions were collected in the region of 400-450 nm. CAF was then quantified using the image processing software Metamorph (Metamorph; Molecular Devices, Sunnyvale, CA). Once imported into the software, three 200 by 200 pixel regions of interest were defined in both the treated and untreated portions of each section. The average pixel intensity of each region was reported by the software as an arbitrary 8 bit value. The three regions within the treated portion were averaged, as well as the three within the untreated portion, the background. The resulting averages were subtracted from each other to obtain an increase in CAF intensity of the treated region in a given section.<sup>27, 31, 32</sup>

### *SDS Page:*

To verify that chemical crosslinking was actually occurring during the NLO CXL treatment compressed collagen hydrogels were treated and run through an SDS Page electrophoresis gel. Rat tail type I collagen (3 mg/ml) was neutralized with 1 N NaOH (Acros, NJ), poured into a 24 well plate and left to polymerize at 37°C in a 5% CO<sub>2</sub> humidified incubator to form a hydrogel. Gels (3 ml each) were then compressed into sheets roughly 150 µm thick as previously described<sup>29</sup> and 2.5 mm diameter discs were taken from each sheet using a trephine. The discs were soaked in riboflavin solution,

0.1% for UVA CXL and 0.5% for NLO CXL, with no dextran for 30 minutes and then mounted and treated in 4.5 by 4.5 mm area in the same manner as described above for ex vivo corneal samples. The focus was aimed at the center of the gel, in all directions, to achieve maximum crosslinking. Treated gels were then solubilized by boiling in Laemmli SDS buffer and the resulting solutions were run through an electrophoresis gel to compare the size of the molecules in the various samples, with crosslinking samples having theoretically larger molecules.

## Results

Figure 4 shows the images taken of the CAF in various corneas. Controls soaked in riboflavin alone showed only background levels of CAF (4A), while control corneas which received UVA CXL for 30 minutes showed increased CAF in the anterior stroma (4B). A cornea which received NLO CXL at the slowest speed, with a line separation of 17.5  $\mu\text{m}$  for visual demonstration of the focal volume is shown in Figure 4C. The highest intensity of the CAF signal was measured in corneas treated with NLO CXL at 2.69 mm/s speed and 4.4  $\mu\text{m}$  line separation (4D) and showed 2.9 times greater signal than that achieved by standard UVA CXL and reached a comparable depth averaging  $182.97 \pm 52.53 \mu\text{m}$  for NLO CXL and  $147.84 \pm 4.35 \mu\text{m}$  for UVA CXL. The line width of the NLO CXL treated eyes was also measured to be 3  $\mu\text{m}$ . These measurements closely match the theoretical calculations for the size of a two photon focal spot in corneal tissue of a 760 nm beam focused through a 0.1 NA objective (Table 1).

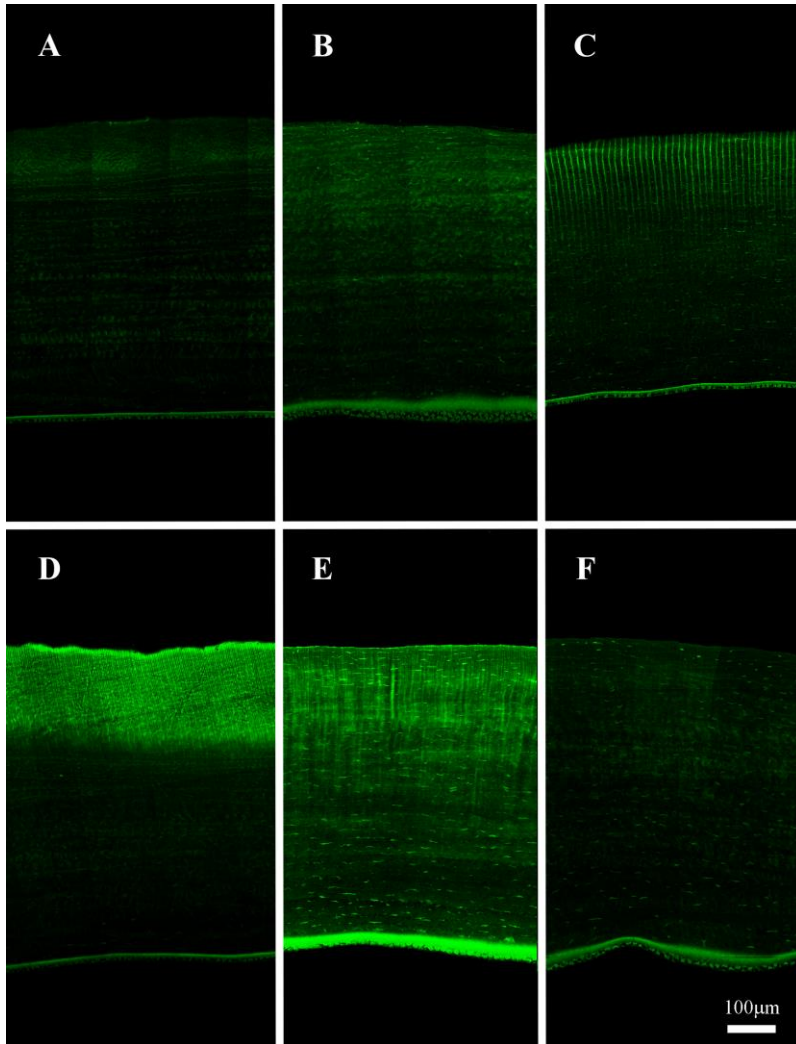


**Figure 4: CAF Images of Corneal Sections**

(A) Control 2, CAF of a cornea treated with epithelial removal and soaked in riboflavin 0.5%, dextran 20%. (B) Control 3, CAF of a cornea treated with the standard UVA CXL protocol. (C-F) Show corneas treated with NLO CXL. The section shown in (C) had a 2.69 mm/s speed (1638.4  $\mu$ s pixel dwell time) and line separation of 17.6  $\mu$ m (all others had a line separation of 4.4  $\mu$ m). The section shown in (D) was also treated with a speed of 2.69 mm/s, (E) with a speed of 5.37 mm/s (819.2  $\mu$ s dwell), and (F) with a speed of 10.74 mm/s (409.6  $\mu$ s dwell). Reprinted/ adapted with permission from the Journal of Cataract and Refractive Surgery.<sup>31</sup>

The arbitrary intensity values, calculated from CAF images are presented in Figure 5. This graph shows a linear decrease in CAF intensity with increasing effective speed with an  $R^2$  value of 0.9689 after linear regression was performed. It was also noted that

NLO CXL CAF intensity approached UVA CXL CAF intensity at a speed of 8.9 mm/s (494  $\mu$ s dwell), suggesting that effective therapeutic crosslinking can be achieved at even faster speeds than the standard UVA CXL treatment allows. At this speed a 3 mm diameter area could be treated in less than 4 minutes.

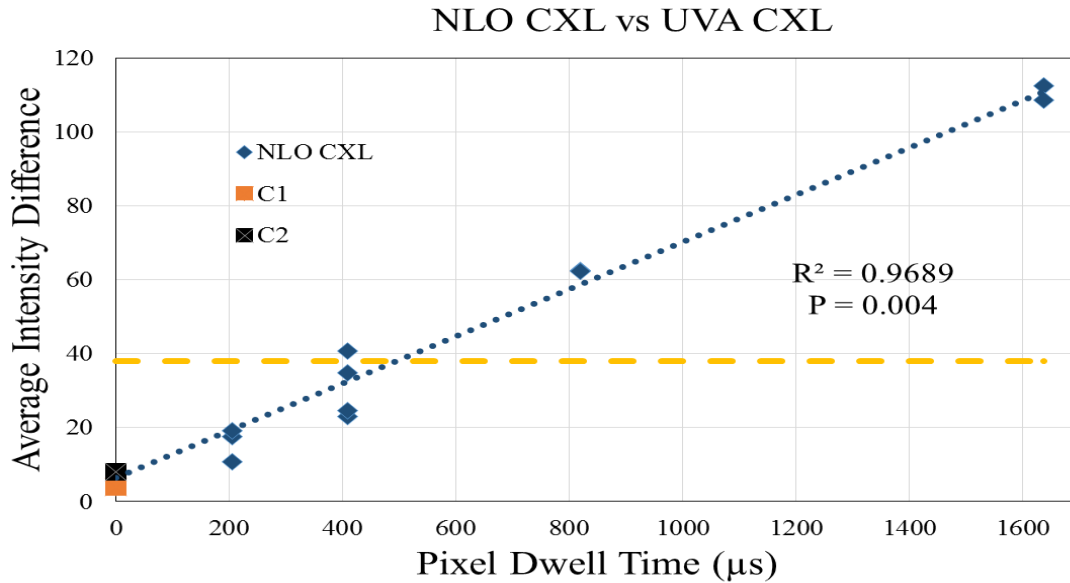


**Figure 5: Average CAF Intensity of UVA vs. NLO CXL**

Mean intensity difference of CAF between treated sections and untreated sections in NLO CXL and UVA CXL. The mean intensity increase, arbitrary units, was plotted for control eyes and treated eyes to compare the effects of increasing dwell time (decreasing scanning speed) on CAF. The data were found to match the line  $y = 0.0636x + 6.5323$  with an  $R^2$  value of 0.9689 and a significance of  $P < 0.05$  between different dwell times. The mean CAF for UVA-treated eyes was plotted as a horizontal dashed line. CAF from NLO CXL exceeds this amount at dwell times greater than 494  $\mu$ s, corresponding to a speed of 8.9 mm/s (C1 = control 1; C2 = control 2). Reprinted/ adapted with permission from the Journal of Cataract and Refractive Surgery.<sup>31</sup>

To further verify these results compressed collagen hydrogels were treated with both the NLO and UVA CXL and run through an SDS page electrophoresis gel as shown in Figure 6. After both UVA and NLO CXL treatments all three collagen bands,  $\beta$ ,  $\alpha 1$  and  $\alpha 2$ , show a visually detectable decrease in intensity. The intensity of the  $\beta$ ,  $\alpha 1$ , and  $\alpha 2$

bands was calculated to be only 10.4%, 26.3%, and 9.1% of the control, lane 1 of 6A, when subjected to 10 minutes of UVA treatment, lane 2 of 6A. NLO CXL treatment at the slowest speed, lane 1 of 6B, had similar results of 8.9%, 41.6%, and 9.3% compared to control. The collagen gels treated at faster speeds, lanes 2 and 3 of 6B, were less affected by the procedure, showing 44.2%, 55.7%, and 81.5% of the control for effective speed of 5.37 mm/s and 27.5%, 52.5%, and 61.4% of the control for effective speed of 10.74 mm/s.

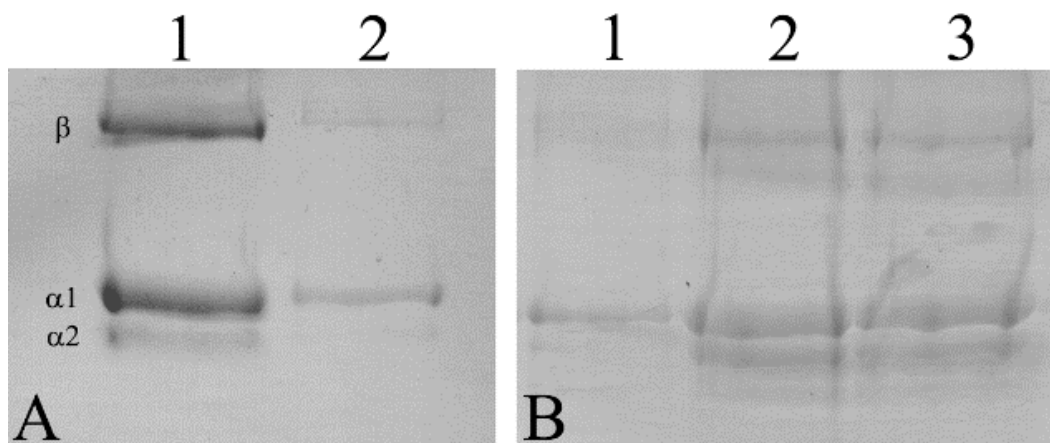


**Figure 6: SDS Page of Compressed Collagen Gel**

**Treated with UVA or NLO CXL**

(A) Shows an SDS page of a compressed collagen hydrogel treated using UVA CXL. Lane 1 shows a control collagen hydrogel, with no CXL. Lane 2 shows a collagen hydrogel treated with UVA CXL for 10 minutes. (B) Shows a collagen hydrogel treated with NLO CXL. Lanes 1, 2, and 3 represent hydrogels treated with increasing effective speeds of 2.69 mm/s, 5.37 mm/s, and 10.74 mm/s, respectively. Reprinted/ adapted with permission from the Journal of Cataract and Refractive Surgery.<sup>31</sup>

**Discussion**

Chai et al.<sup>29</sup> showed that multiphoton activation of riboflavin using focused 760 nm fs laser light through a 0.75 NA lens produces comparable mechanical stiffening of collagen hydrogels to that shown of standard UVA CXL using 370 nm light. The high NA, however, produces crosslinking in a very small volume, 0.5  $\mu\text{m}$  lateral and 2.5  $\mu\text{m}$  axial.

While this increases the precision, potentially addressing the limitations of UVA CXL, the length of the procedure is impractical for a clinical setting.

This study shows that it is possible to achieve a similar degree of crosslinking by using a low NA lens that produces a focal volume three orders of magnitude larger. Using a 0.1 NA lens, single pass NLO CXL induced greatly enhanced CAF within ex vivo rabbit corneas that was of equal depth in the cornea compared to standard UVA CXL. Chemical data also verified the ability of NLO CXL to induce molecular crosslinking of collagen molecules as evidenced by the loss of individual collagen  $\alpha 1$  and  $\alpha 2$  chains that form the triple helical collagen molecule upon polymerization. Zhang et al.<sup>34</sup> demonstrated that collagen subjected to UVA CXL showed a marked decrease in the amount of  $\alpha$  and  $\beta$  chains when subjected to gel electrophoresis. In this study, SDS page electrophoresis gel was performed with both an untreated control and a standard UVA treated gel for comparison. Since crosslinking of the collagen results in much larger molecules, the smaller molecules, clearly visible in the untreated control collagen hydrogel, are fewer or nonexistent in crosslinked collagen. This suggests that following NLO CXL, covalent bonds form between  $\alpha 1$  and  $\alpha 2$  chains creating larger molecular weight molecules that are unable to migrate into the gel. It should be noted that no NLO CXL gel showed as much decrease in  $\alpha 1$  and  $\alpha 2$  as a gel treated with the full 30 minutes of UVA CXL. This is likely due to the untreated portions of gel around the edges of the NLO CXL area. It is possible to treat the full area of a gel with UVA CXL, but not with NLO CXL using this set up.

With these experiments we demonstrated that a larger focal volume provides for rapid NLO CXL. This provides proof of concept for NLO CXL as a technique and

justification for building a custom crosslinking device of our own design, separate from the Zeiss microscope, which has the ability to continuously vary focal volume size, depth within the cornea, and pattern of crosslinking.

## Chapter 2: Custom Built NLO CXL Device

### Introduction

Previous studies have shown that it is not only possible to mechanically stiffen collagen hydrogels to a degree similar to that achieved by standard UVA CXL using NLO CXL,<sup>29</sup> but that it is also possible to effectively, and rapidly crosslink ex vivo rabbit corneas.<sup>31</sup> As presented in Chapter 1, a similar degree of enhanced CAF, used as a measure of collagen CXL, can be detected in ex vivo rabbit corneas treated with both NLO CXL and UVA CXL, depending on the scanning parameters.<sup>31</sup> In these studies a Zeiss LSM 510 confocal microscope (Carl Zeiss, Jena, Germany) was used to perform NLO CXL. While it was effective, a higher degree of control is needed over parameters such as NA, scanning speed, scanning pattern, line separation, etc. This chapter focuses on the design, construction, and initial testing of a customized device with a higher degree of control over these variables which is capable of delivering a nonlinear focal volume into both ex vivo and in vivo rabbit corneas.

### Materials and Methods

#### *Device Design:*

A device capable of delivering a nonlinear focal volume of continuously variable size into rabbit corneas was built, according to the design seen in Figure 7. In this design, the 760 nm fs beam (Chameleon, Coherent Inc.) is directed into a variable beam expander which allows for control of the effective NA of the device, and therefore control of the size of the focal volume. For example, when the beam is fully widened it completely

fills the back aperture of the objective producing the highest NA and smallest focal volume. The widened beam is then directed onto software controlled x, y scanning mirrors (GSI Lumonics, Bedford, MA) which scan the focal volume through a preprogrammed pattern. A second fixed beam expander widens the beam again before it hits the back aperture of the objective. Depth is controlled by a computerized motor on the objective by moving the focusing lens up and down. A removable cone with contact glass flattens the cornea during treatment, stabilizing the eye and establishing a zero plane.

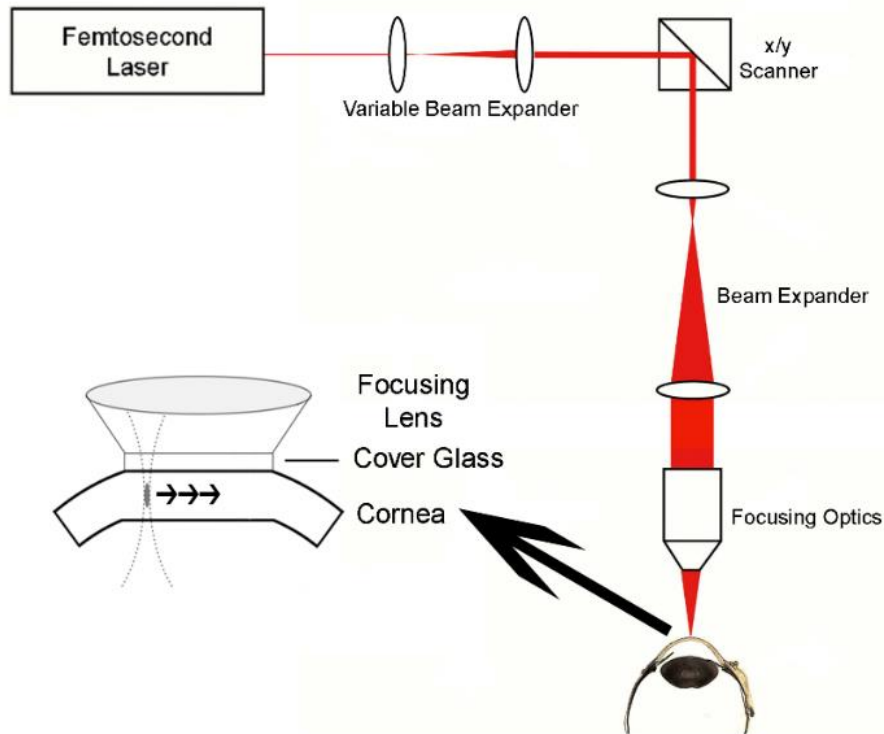


**Figure 7: Design of NLO CXL Delivery**

Schematic of designed delivery device with software controlled x, y scanners, variable beam expander, and objective with attached cone and contact glass. Reprinted/ adapted with permission from Biomedical Optics Express.<sup>32</sup>

### *Effect of NA on Focal Volume:*

After the delivery device was designed and ready for use, the effect of NA on focal volume size was characterized. The effective NA of the system was calculated for five designated positions of the variable beam expander, labeled 1-5. A tank of 0.5% riboflavin-5-phosphate solution (Sigma-Aldrich, St. Louis, MO) in PBS (pH 7.2) was placed beneath the objective and raised to the focal plane level, so that a fluorescent focal volume would be visible within the solution. A SPOT RT3 camera (SPOT Imaging Solutions, Sterling Heights, MI) with an attached 10X objective was positioned in front of the tank and images were taken of the riboflavin fluorescence by all five beam expander positions using an IR blocking filter. The pixel size of the resulting images was 0.74  $\mu\text{m}$ . Within each image a line was drawn axially and laterally using Metamorph digital image processing software (Metamorph; Molecular Devices) through the focal volume. Intensity values along these lines were exported into Excel and plotted as intensity vs. distance. Full width half max (FWHM) values were calculated using these plots to estimate the lateral and axial dimensions of the focal volume at each setting. Axial measurements were then used to calculate the effective NA based on Zipfel's equations<sup>30</sup> shown in Eq (1-3), where  $\omega_z$  is axial length of the focal volume,  $\omega_{xy}$  is the lateral width,  $V$  is the volume of the focal spot,  $\lambda$  is the excitation wavelength, and  $n$  is the refractive index of the surrounding medium. Images were also taken as the depth was increased in steps to estimate the maximum depth available.

$$\omega_z = \frac{0.532\lambda}{\sqrt{2}} \left[ \frac{1}{n - \sqrt{n^2 - NA^2}} \right] \quad (1)$$

$$\omega_{xy} = \begin{cases} \frac{0.32\lambda}{\sqrt{2}NA}; & NA \leq 0.7 \\ \frac{0.325\lambda}{\sqrt{2}NA^{0.91}}; & NA > 0.7 \end{cases} \quad (2)$$

$$V = \pi^{3/2} \omega_{xy}^2 \omega_z \quad (3)$$

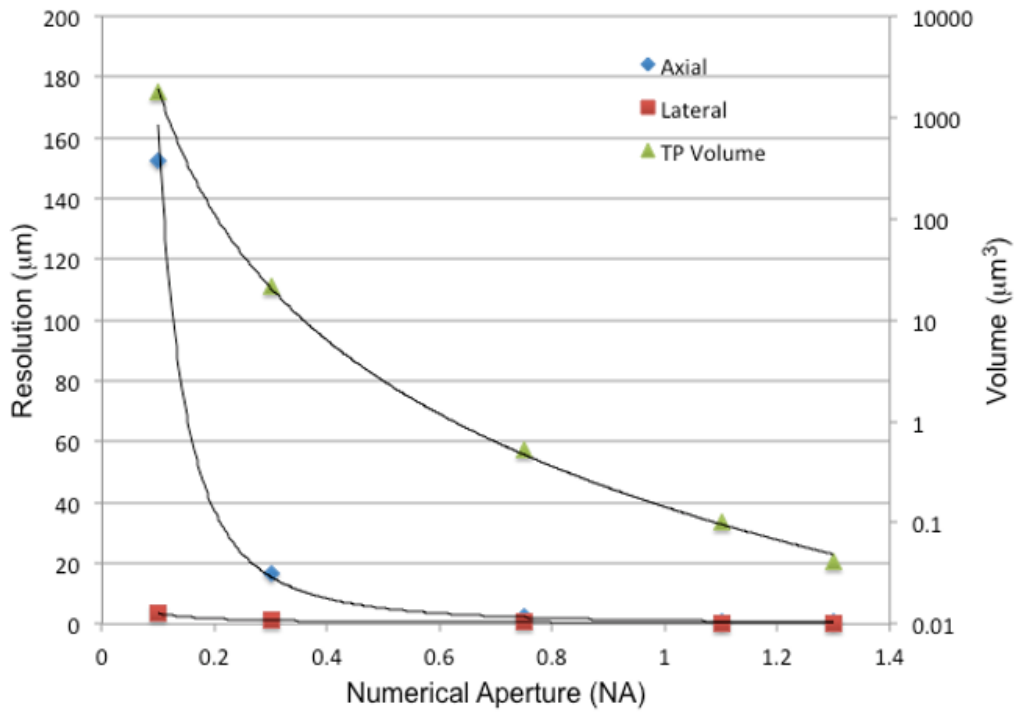


**Figure 8: NA vs. Focal Spot Size**

Graphs of theoretical axial and lateral dimensions and volume with respect to NA calculated using Zipfel's equations (1-3).<sup>30</sup>

It should be noted that these measurements also depend on other specific parameters outside the control of just the telescope, such as the diameter of the incoming beam. If the alignment of the optics into the delivery device are altered, so too are the

measurements presented here, though the same equations hold. While a consistent alignment was maintained for the experiments in this chapter, allowing us to assign a specific NA value to each telescope setting, the alignment had to be altered for later experiments making the NA values listed here unreliable in all other chapters.

### *Preparation of Eyes:*

Eyes were prepared in the same manner as in Chapter 1. Briefly, whole New Zealand albino rabbit eyes (71) were shipped overnight to the laboratory (Pel-Freez, Rogers, AR) for immediate use. Eyes were inspected for damage and marked for orientation before having the corneal epithelium removed in an 8 mm diameter region of the central cornea. Drops of 0.5% or 0.1% riboflavin-5-phosphate solution, for NLO CXL or UVA CXL respectively, with 20% high-fraction dextran, molecular weight of 450-650 KDa, (Sigma-Aldrich, St. Louis, MO) in PBS were applied every two minutes for 30 minutes, in the manner outlined by Spoerl and Wollensak.<sup>6, 7</sup>

### *Treatment of Eyes:*

A total of 71 eyes were divided into 4 different experimental groups. Eighteen eyes were treated with NLO CXL using a variable beam expander setting of 1, with total power of either 900 mW (12) or 500 mW (6). The NA at this setting was measured to be 0.12, the closest reliable setting to our previous studies using the Zeiss confocal microscope, which used a NA of 0.1.<sup>31</sup> These 18 eyes were then placed underneath of the objective of the delivery device with the positioning mark placed to the far left and the pupil aligned

in the center of the contact glass. The corneas were then exposed to 760 nm fs laser light at 900 mW or 500 mW of power, with the center of the focus positioned 50  $\mu\text{m}$  below the corneal surface. Using custom Labview software the beam was raster scanned over a 4 mm diameter circular area at 5.4 mm/s and 3  $\mu\text{m}$  line separation. This resulted in a cylindrical volume of treated area of approximately 1.4  $\text{mm}^3$ . Total exposure time for each NLO CXL treatment was roughly 11 minutes. For comparison, the remaining eyes were used as controls (38), with no soaking and no treatment, or were treated with UVA CXL (15) using 370 nm excitation at 3  $\text{mW}/\text{cm}^2$  for 30 minutes, as before.<sup>31</sup>

### *Mechanical Measurements:*

After treatment, eyes were prepared for mechanical stiffness testing using the indentation approach described by Chai et al. and Levental et al.<sup>29, 35</sup> An indentation approach was used because of the need to measure local tissue stiffness in the region of NLO CXL. Specifically, indentation allows for mechanical stiffness testing in a 1 mm diameter region whereas more standard tensiometry or stretch testing would require using a strip of cornea, for which much of the tissue would have been un-crosslinked. A 5 x 5 mm area of cornea, centered on the pupil was removed from the globe and its thickness measured using a pachymeter (Reichert Technologies, Depew, NY). Corneal thickness was then adjusted to within 400-450  $\mu\text{m}$  by dropping either PBS to thicken or 20% dextran solution to thin the cornea. It was necessary to control thickness because the dextran solution used on treated eyes caused marked corneal thinning, which could make them appear to be artificially stiffer than control corneas. Preparation for mechanical measurements took roughly 30 minutes for each sample. Each excised portion of cornea

was then placed directly under a 1 mm diameter, flat tip probe with attached force transducer which was manually moved down to contact the anterior surface of the tissue, as shown in Figure 9. The probe was then cycled up and down ten times at a rate of 5  $\mu\text{m/s}$ , indenting up to 10% of the measured thickness. Equations outlined initially by Hayes et al.<sup>1, 35-37</sup> were used to convert the force value reported at the peak of the tenth cycle to elasticity measurements of the corneal sample (Eq 4). In this equation the variable  $\nu$  represents poisson's ration for corneal tissue which is assumed to be 0.49.<sup>1, 38</sup> The depth of indentation, 10% of the measured corneal thickness, is represented by the variable  $\omega$ . The correction factor  $\kappa$ , based on the ratio of the indentation probe's radius and corneal thickness was 3.29 for all samples. The radius of the indentation probe,  $\alpha$ , was 0.5 mm, and  $F$  is the force measured by the probe in mN. Damaged eyes or inability to find the treated area before dehydration occurred forced the omission of mechanical measurements on 2 control eyes, 2 UVA CXL treated eyes, 1 900 mW NLO CXL treated eye, and 2 500 mW NLO CXL treated eyes. Also seven control eyes were used only for CAF analysis, and did not undergo mechanical testing. Elasticity values were obtained on a total of 29 control eyes, 13 UVA CXL treated eyes, 11 NLO CXL eyes treated with 900 mW, and 4 NLO CXL eyes treated with 500 mW. After measuring the stiffness, corneas were fixed overnight in 2% paraformaldehyde (PFA, Mallinckrodit Baker, Inc., Phillipsburg, NJ) in PBS at 4° C.

$$E = \frac{(1-\nu^2)F}{2\alpha\kappa\omega} \quad (4)$$

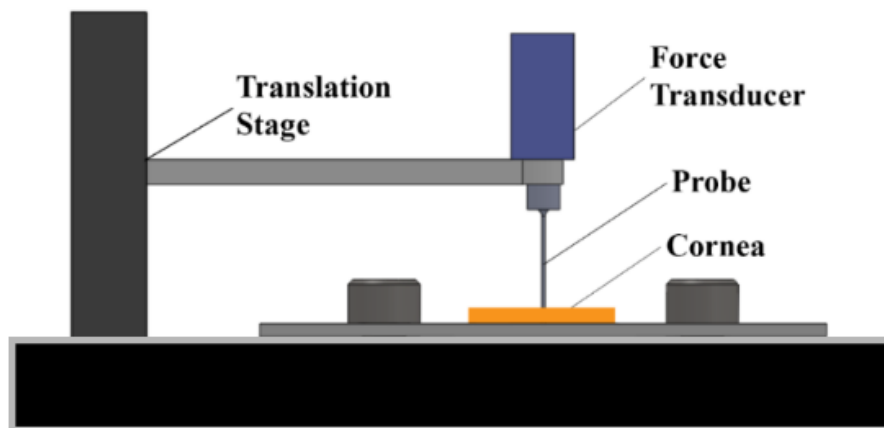


**Figure 9: Design of Mechanical Indentation System**

Schematic of indentation device used to measure the mechanical stiffness of the corneal stroma. Reprinted/ adapted with permission from Biomedical Optics Express.<sup>32</sup>

### *Sectioning and Imaging:*

Fixed corneas were sectioned and imaged for CAF as described in Chapter 1. Intensity differences were then measured within 12 bit images of each sample, as before,<sup>31, 32</sup> (one section per eye) using Metamorph imaging software to calculate the average intensity value within three different 100 x 100 pixel regions of interest within the crosslinked region (central anterior). Average intensities of the crosslinked region were compared to intensities from the same location of control eyes. Three NLO CXL samples were not able to be sectioned perpendicularly due to error in orientation during treatment and were excluded from CAF measurements. Four UVA CXL samples were also excluded due to improper sectioning. In this report CAF intensity is reported in a total of 7 control eyes, 11 UVA CXL treated eyes, and 15 NLO CXL treated eyes (10 at 900 mW, 5 at 500 mW).

Statistical analysis was performed in all cases using the Tukey-Kramer method for a multiple comparison, one-way analysis of variance (ANOVA) in Matlab (Mathworks, Natick, MA).

## Results

### *Control of Focal Volume and Depth:*

Two-photon excited fluorescent images of riboflavin taken with the SPOT RT3 camera are shown in Figure 10, and demonstrate control of fluorescent focal volume (10A) and depth (10B). To determine the NA of different beam expander settings, the lateral and axial lengths FWHM were measured. These empirical values were then used to calculate the focal volume and effective NA of each setting using the theoretical equation, (Eq 1).<sup>30</sup> As quantified in Table 1, changes in the beam expander setting had a dramatic effect on both axial length and focal volume, such that increasing the beam expander setting from its minimum to maximum position, 1-5, produced a more than 7.5 fold change in volume and 2.5 fold change in axial length, Figure 11. As the beam expander setting increased from 1 to 5 the axial FWHM length decreased from 79.5  $\mu\text{m}$  to 28.6  $\mu\text{m}$ . Using Zipfel's equation (Eq 1)<sup>30</sup> this would correspond to a range of 109.5  $\mu\text{m}$  to 39.5  $\mu\text{m}$  in corneal tissue for corresponding NA's. The lengths are increased in corneal tissue compared to water because the refractive index of corneal tissue is 1.376, larger than that of water, 1.33. A range of depth of up to 500  $\mu\text{m}$  below the contact glass was also reached (10B).

**Table 1. Calculated Axial and Lateral Length, Focal Volume, and NA<sup>32</sup>**

Beam Expander Setting	FWHM ( $\mu\text{m}$ )		Volume ( $\mu\text{m}^3$ )	Theoretical volume in Cornea ( $\mu\text{m}^3$ )	Calculated NA
	Axial	Lateral			
1	79.5	2.9	1407.1	1939.4	0.12
2	59.9	2.5	800.7	1104.3	0.14
3	41.0	2.3	375.6	518.6	0.17
4	36.3	2.2	294.9	407.3	0.18
5	28.6	2.5	182.8	252.8	0.20

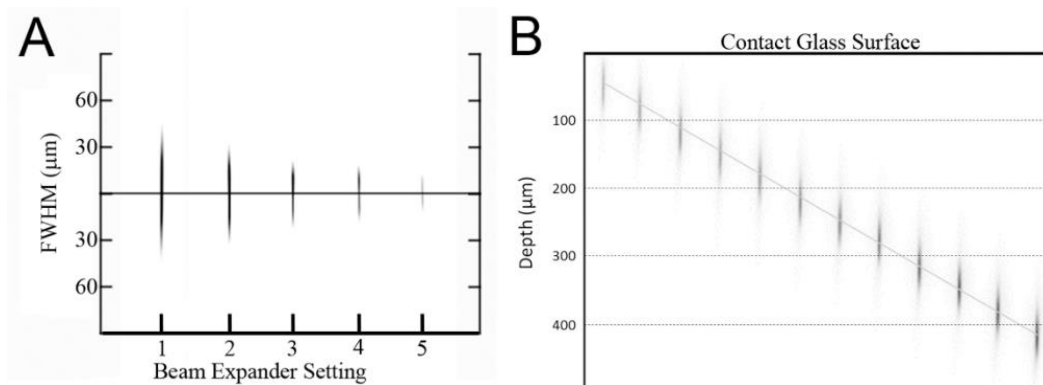


**Figure 10: Images of Focal Volume**

Images taken of the two photon focal volume in a tank of riboflavin solution as the beam expander setting (A) and depth (B) were increased in steps, used to measure the size of the focal volume and depth below the contact glass. Reprinted/ adapted with permission from Biomedical Optics Express.<sup>32</sup>

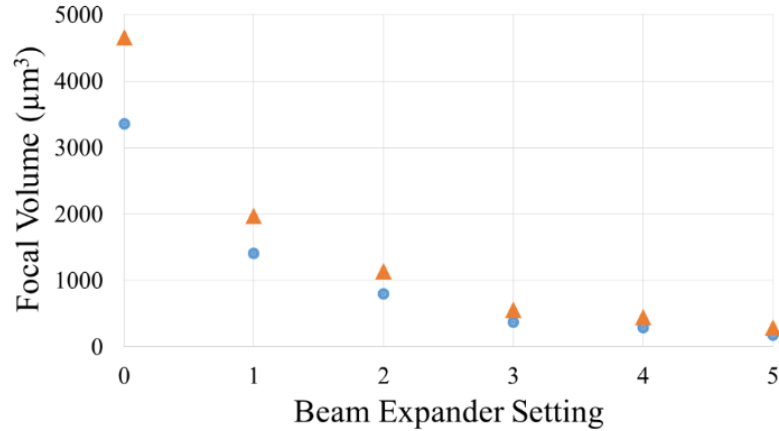


**Figure 11: Beam Expander Setting vs Focal Volume**

As the beam expander setting increased, the volume of the focal spot decreased more than 18 fold in both water (blue circles) and corneal tissue (orange triangles). Reprinted/ adapted with permission from Biomedical Optics Express.<sup>32</sup>

### *Change in Mechanical Stiffness:*

An example indentation measurement is shown in Figure 12. As the probe moved deeper into the normal corneal tissue (blue), the force reported by the transducer, in mN, increased, and moving the probe out of the tissue resulted in decreasing force measurement, which was lower at every value due to hysteresis of the tissue. By comparison, indentation of corneal tissue treated with NLO CXL (orange) showed increased peak force compared to control corneas indicating mechanical stiffening. The value used for calculations was the force value taken at the peak of the tenth cycle, at 10% strain.

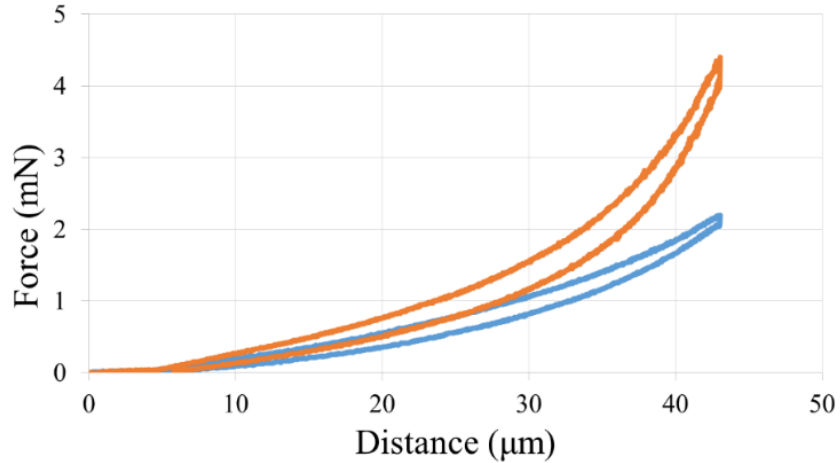


**Figure 12: Force Required to Indent the Stroma**

Plotted force required to indent the corneal stroma to 10% thickness. The orange graph shows the data for a single indentation cycle of a sample crosslinked with 900 mW, and the blue graph shows the same data for a control cornea. Reprinted/ adapted with permission from Biomedical Optics Express.<sup>32</sup>

Figure 13 shows the results from the force measurements converted, using Eq (4), to the elastic moduli for control, UVA CXL, and NLO CXL samples. Both UVA CXL (green) and 900 mW NLO CXL (blue) samples were shown to be significantly stiffer than controls (black) with P values of less than 0.001 (Power = 0.9 for a twofold difference between NLO CXL and control, and 0.8 for a twofold difference between UVA CXL and control). Comparison of the elasticity measured for NLO CXL was not significantly different from that obtained following UVA CXL (P=0.66). Corneas treated with 900 mW NLO CXL (11) had an average elasticity of  $25.95 \pm 8.23$  KPa, 2.6 times the  $9.91 \pm 4.54$  KPa of the control corneas. In comparison, corneas treated with UVA CXL (13) had an elasticity of  $28.72 \pm 12.11$  KPa on average, 2.9 times the force needed to indent control corneas. The samples treated with 500 mW NLO CXL (4) had an average elasticity of  $12.21 \pm 4.12$  KPa, 1.2 times higher than control, though not significantly higher.

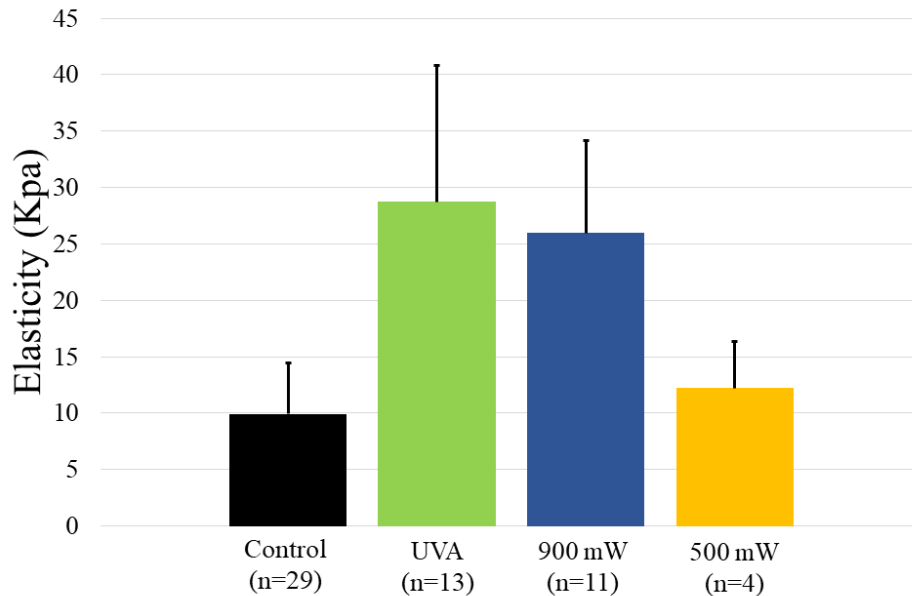


**Figure 13: Corneal Elasticity after CXL**

Both UVA (green) and 900 mW NLO (blue) treated eyes were significantly stiffer than controls (black) with P values less than 0.001. Reprinted/ adapted with permission from Biomedical Optics Express.<sup>32</sup>

### *NLO CXL Induced CAF:*

A correlation between CAF and mechanical stiffness was demonstrated in Chapter 1.<sup>31</sup> Images of CAF showed a similar intensity of emission for NLO CXL treated eyes as achieved by UVA CXL. Figure 14 provides examples of CAF images used to take intensity measurements. As shown in Figure 15 the average intensity per  $0.4 \mu\text{m}^2$  area of eyes treated with UVA CXL (10), 900 mW NLO CXL (10), and 500 mW NLO CXL (5) were  $2603.61 \pm 490.47$ ,  $2717.78 \pm 403.01$ , and  $2423.54 \pm 222.31$  respectively in the anterior crosslinked stroma compared to an intensity of  $409.47 \pm 10.14$  in the comparable anterior stroma of control eyes. No significant difference was seen between the intensities of any

of the treatment groups,  $P = 0.6$ , but all groups were significantly brighter than controls,  $P < 0.001$ . The statistical analysis had a power of 0.86 for a 30% difference.

Note: Intensity values for CAF in this chapter are higher than those listed in Chapter 1 because 12 bit images were used in this study, as opposed to the 8 bit images used previously. Also, instead of subtracting background intensities within each individual image, anterior intensities were compared to intensities of control samples. This was done to avoid using any areas that were too close to the CXL area, which might have had slightly increased CAF in some UVA CXL samples.

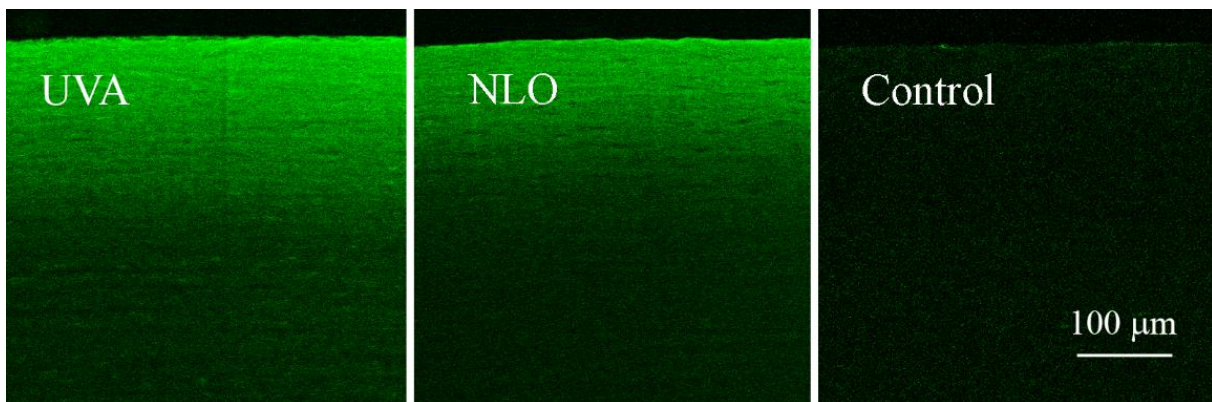


**Figure 14: Corneal CAF after CXL**

Examples of CAF images for UVA CXL, NLO CXL (900 mW), and control samples. Reprinted/ adapted with permission from Biomedical Optics Express.<sup>32</sup>

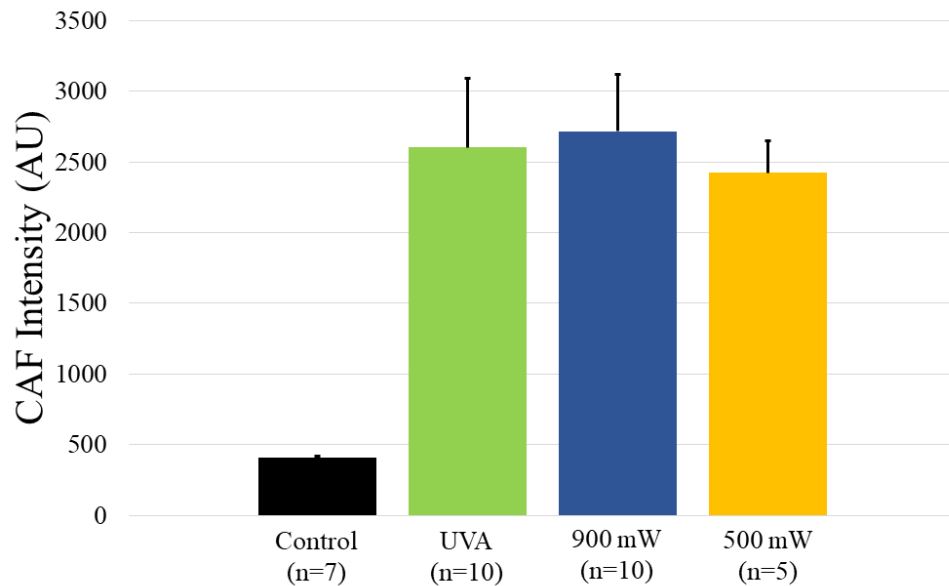


**Figure 15: CAF Intensity after CXL**

CAF intensity was not significantly different between UVA (green) or NLO (blue, yellow) treatment groups. Reprinted/ adapted with permission from Biomedical Optics Express.<sup>32</sup>

## Discussion

It was shown in Chapter 1 that a low NA lens (0.1) can generate a CAF signal in ex vivo rabbit eyes that has an expanded axial and lateral dimension suggesting a dramatic increase in crosslinking volume compared to the high NA lenses used by Chai et al.<sup>29, 31</sup> This increased CAF volume suggests that by using a low NA lens one might be able to use NLO CXL to more rapidly and precisely crosslink large volumes of cornea to increase tissue mechanical stiffness. For this study we designed a custom device which allows control over lens NA, focal volume size, depth within the cornea, scanning speed, and pattern of crosslinking, in ex vivo or in vivo eyes.

In this study we demonstrated that NLO CXL treatment using this device is capable of mechanically stiffening, and increasing the CAF intensity of corneal tissue comparably to UVA CXL treatment. Corneas treated with NLO CXL, using 900 mW of laser power, were significantly stiffer than controls. In fact, the elasticity of these samples was 2.6 fold higher than that of control samples, comparable to the 2.9 fold increase following UVA CXL. Also all three treatments showed a similar increase in CAF intensity of the treated region. This suggests that the lack of significant increase in elasticity of 500 mW NLO CXL group may be partially due to the small sample size or lack of sensitivity of the indentation method. While this study showed potential for this NLO CXL design, there was much that still needed to be improved upon.

Some improvements may be made simply by experimenting with the pattern of crosslinking. The versatility of focal volume size and placement allows for more regionally defined crosslinking. For example, this technique could allow for crosslinking of the area around the LASIK flap as a preventative measure against post LASIK ectasia. This versatility could also be used to design customized treatment patterns for Keratoconus patients based on their corneal topography and regional thickness. Also, since crosslinking treatment has been shown to flatten corneas as much as one-two diopters, modifying corneal shape using NLO CXL may have the potential to correct refractive errors.<sup>16, 17</sup>

In conclusion, a device was developed that provides for NLO CXL of the cornea that is as effective for mechanical stiffening of the corneal stroma as UVA CXL. Further development of this novel technology may help expand the applicability domain for corneal crosslinking by providing for faster, safer, and more controlled regional stiffening.

### *Issues:*

One obstacle of this initial system was the total power being used. The laser that was used as a source for this device, a 80 MHz laser, required a full 900 mW of laser power using a 0.1 NA lens and thousands of overlapping pulses to achieve a desirable crosslinking effect. The American National Standards Institute (ANSI) retinal thermal power limit for 760 nm fs light focused with a 0.1 NA lens was calculated using Eq 5-7.<sup>39</sup> In these equations  $W$  represents the maximum thermal power allowed in watts,  $t$  is the exposure time of the procedure,  $P$  (pupil factor) is equal to 1, and  $\alpha$  (visual angle) is equal to 200 mrad. For a 760 nm wavelength the maximum allowable exposure was calculated to be 46.1 mW, well below the 900 mW used in this study. For this reason a switch to amplified pulses was necessary to develop a clinically applicable technique (Chapter 5). The increase in pulse energy using a repetition rate in the kHz range (as opposed to the 80 MHz laser) allows for a dramatic decrease in the overall power, satisfying ANSI limits and reducing the need for overlapped pulses. Use of regeneratively amplified fs lasers has the potential to overcome a major hurdle toward the clinical applicability of NLO CXL. The initial plan was to use the Legend-F Titanium Sapphire Regenerative Amplifier System (Coherent) available in Dr. Juhasz's laboratory. This system is a 5 kHz, 130 fs pulsed laser that can deliver 1.25 W at an 800 nm wavelength. However, the 800 nm wavelength did not produce the desired CXL effects. Altering the system to deliver a 760 nm beam was possible, but proved difficult and unstable. For this reason a custom laser system was designed which is capable of producing a 760 nm, amplified fs pulse beam (for more detail, see Chapter 5).

$$W = (6.93 * 10^{-4})C_E C_T P^{-1} t^{-0.25} \quad (5)$$

$$C_E = (6.67 * 10^{-3})\alpha^2 \quad (6)$$

$$C_T = 10^{0.002(\lambda-700)} \quad (7)$$

Another issue with this setup is that it is impossible with our current method to see by eye where the cornea had been treated or in exactly what direction the lines were scanning prior to fixation and imaging. Many sections showed patchy or inconsistent CAF, leading us to believe that we missed the CXL region when cutting out the cornea and therefore did not indent the proper spot during mechanical testing. This forced the exclusion of several data points. Increasing the diameter of the treated region would fix this issue, but it would introduce many more issues such as the possibility of the eye drying or riboflavin leaching out of the cornea due to increased procedure time.

Another major issue involves the indentation method used to measure mechanical properties of the cornea. Not only does this method require pre manipulation of the tissue, allowing the tissue time to dry, it is also somewhat unclear what effect the uncrosslinked posterior region has on the measurements. And, as stated above, it is impossible to tell if the probe is fully in contact with the crosslinked region. To explore this issue we used the indentation device to test the mechanical properties of ten and fifteen percent, 750  $\mu\text{m}$  thick acrylamide gels. Four different combinations of the gels were tested, two layers of 10 %, two layers of 15 %, a layer of 15 % on top of a layer of 10 %, and the reverse to simulate a cornea which has been crosslinked for only half of its thickness. As shown in Figure 16, a significant decrease was seen in the amount of force needed to indent the combination samples ( $P < 0.01$ ), even though the stiffened region was half the total

sample. This indicated that our attempts to measure a stiffened region less than one quarter the entire sample may be getting lost in noise, especially if the crosslinked region is not on the corneal surface. This may explain why samples treated with 500 mW showed increased CAF without stiffening. For this reason lower powers were not excluded from consideration in later experiments.

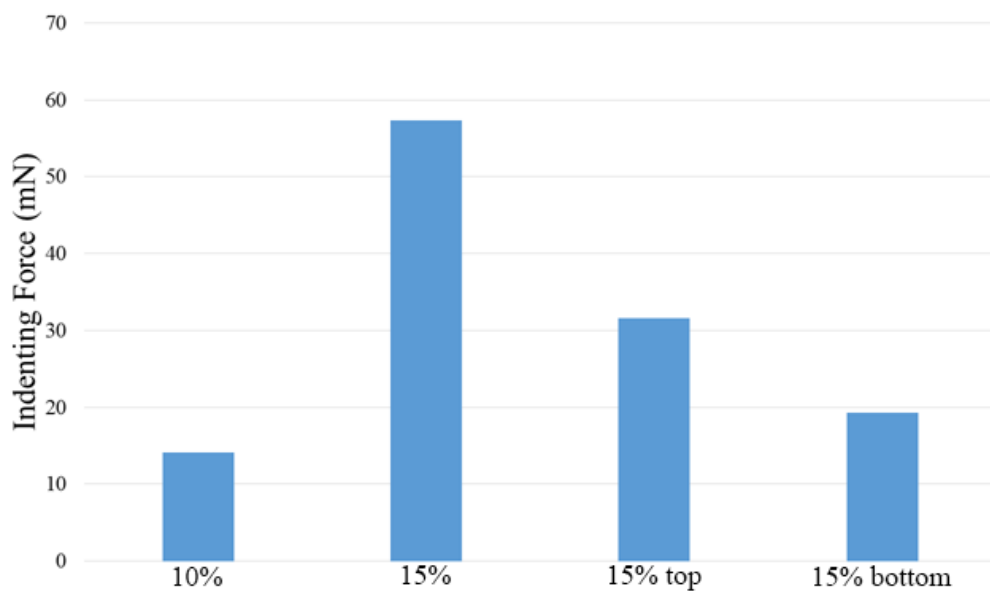


**Figure 16: Stiffness of Acrylamide Gels**

The indentation method was tested on four acrylamide gels, a 1.5 mm thick 10% gel, a 1.5 mm thick 15% gel, a 0.75 mm thick 15% gel on top of a 0.75 mm thick 10% gel and vice versa.

# Chapter 3: Preliminary In Vivo Study

## Introduction

Limited preliminary in vivo experiments were performed to explore the effects of NLO CXL, using non-amplified MHz pulses, in vivo. This study also served to refine the techniques for in vivo monitoring used in later studies.

## Materials and Methods

### *Animals:*

All animals were treated according to the ARVO statement on the use of animals in vision research and experiments were approved by the IACUC of the University of California, Irvine. A total of 5 New Zealand Albino rabbits were treated, one with UVA CXL, one with epithelial debridement only, one scraped and soaked in 0.5% riboflavin, 20% dextran solution, and two treated with NLO CXL at 900 mW, 0.1 NA, 50  $\mu\text{m}$  depth, 2  $\mu\text{m}$  line spacing, and 5.4 mm/s scan speed. Five pigmented rabbits were also treated, one left as a control, three treated with NLO CXL at 500 mW, 0.1 NA, 50  $\mu\text{m}$  depth, 2  $\mu\text{m}$  line spacing, and 5.4 mm/s scan speed, and one where the line separation was increased to 3  $\mu\text{m}$ .

Prior to treatment each rabbit was sedated via a subcutaneous injection of 30-50 mg/kg ketamine hydrochloride (Hospira, Irvine, CA) and 5-10 mg/kg xylazine (Akorn, Lake Forrest, IL). Each animal then received a drop of topical ophthalmic 0.5% tetracaine hydrochloride (Alcon, Ft. Worth, TX) to prevent pain during treatment. After the procedure each rabbit was given 1 ml (0.3 mg/ml) of buprenorphine hydrochloride (Reckitt Benckiser

Healthcare Ltd., UK) to ease pain. Each rabbit was treated with a drop of 0.3% gentamycin sulfate (Allergan, Inc., Irvine, CA) in the treated eye three times daily for three days post treatment to prevent infection.

### *In Vivo CMTF Imaging:*

In vivo confocal microscopy through focus (CMTF) imaging was performed on the right cornea of all rabbits (sedated as described above for the duration of imaging) prior to treatment and at intervals throughout healing to provide measurements of epithelial and stromal thickness, and severity of scattering within the stroma (corneal haze). CMTF is a well-developed technology that has previously been used to monitor corneal wound healing in vivo.<sup>40-42</sup> Briefly, a series of XY plane images through the entire depth of the cornea was captured and a 3D reconstruction of those images provided an in vivo cross sectional view of the cornea, as seen in Figure 17. A graph was then made for each image by plotting intensity versus depth, 17B. Peaks of intensity represent natural structures such as the epithelium, the beginning of the stroma, and the endothelium. Epithelial and stromal thickness were calculated by measuring the distance between intensity peaks. A measure of corneal haze was obtained by calculating the area under the curve in the stromal region. Imaging of treated eyes was repeated at one week, two weeks, one month, and two months post procedure to monitor the wound healing response in the treated region.

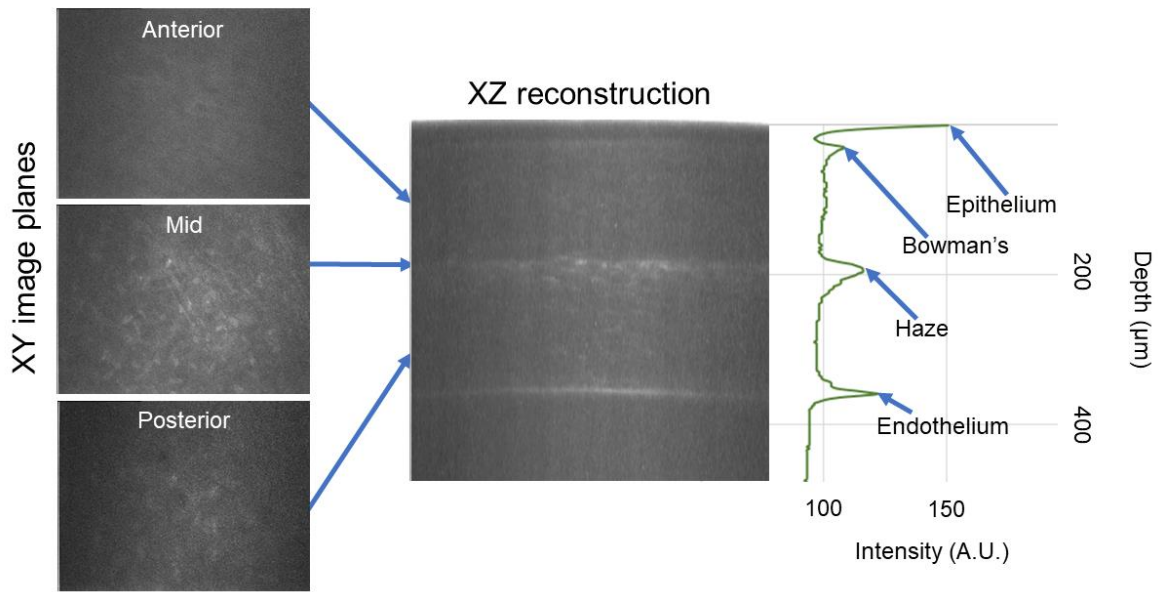


**Figure 17: Example CMTF Image**

The reconstruction and analyzation process of CMTF imaging is shown from left to right. First example XY plane images are shown in the anterior, mid, and posterior stroma. A Full thickness stack of these images is used to create an XZ reconstruction. Finally, Intensities through the depth of the stack are plotted with peaks representing important landmarks such as the epithelium.

### *Mechanical Testing:*

After two months, rabbits were sacrificed and the treated area of each cornea was excised for mechanical testing. Each rabbit was first sedated using 1.5-2 ml of the same ketamine/xylazine cocktail used previously. When fully asleep 1.5 ml (100 mg/kg) of pentobarbital (VEDCO inc., St. Joseph, Mo) was injected as quickly as possible into the marginal ear vein. The cornea was then carefully cut out of the globe, and trimmed down to only the central portion containing the treated area and prepared for indentation testing. The indentation method of mechanical testing described in Chapter 2 was performed in multiple locations so as not to miss the treated region. All corneas were then fixed,

sectioned and imaged in the same manner as previous ex vivo eyes to compare the mechanical results to CAF data.

## **Results**

### *CMTF:*

Examples of CMTF images taken from the albino rabbits prior to the experiment, and one and two weeks post experiments are shown in Figure 18. In both the UVA CXL and NLO CXL treated eyes these images show an acellular region in the treated area followed by a region of high scattering at one week. At two weeks, with both treatments there is high scattering seen throughout the treated region. Figure 19 shows measurements calculated using these scans. Since CMTF images of the first two NLO CXL albino rabbits, treated using 900 mW of laser power, showed a large cellular reaction and scattering in the corneal stroma even past the first month of recovery, the power was decreased to 500 mW to treat the pigmented rabbits. CAF results from ex vivo experiments, detailed in Chapter 2, indicated that this was still enough power to induce crosslinking.

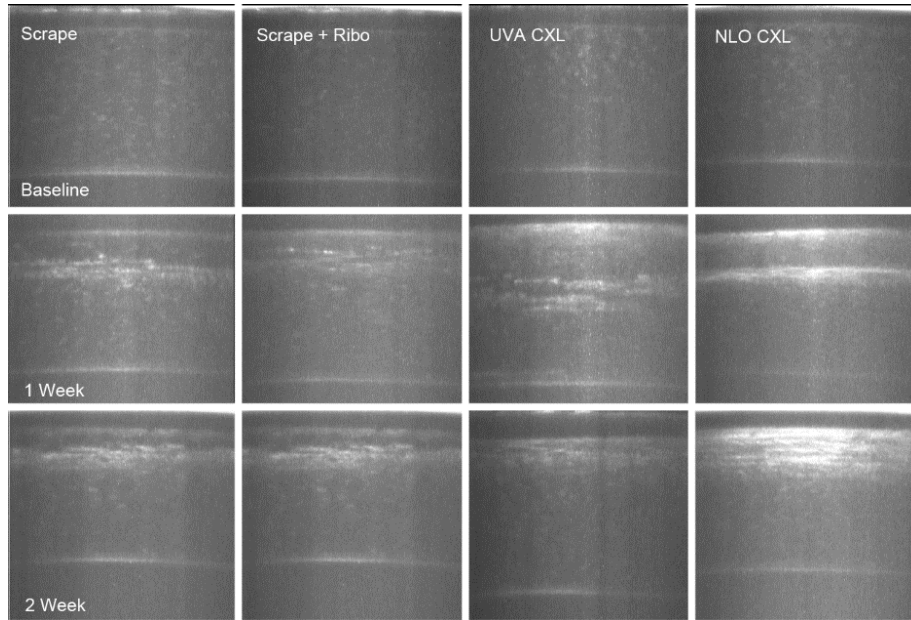


**Figure 18: CMTF Images of Initial In Vivo Study**

CMTF images of the different experimental groups prior to the experiment and at 1 and 2 weeks post experiment.

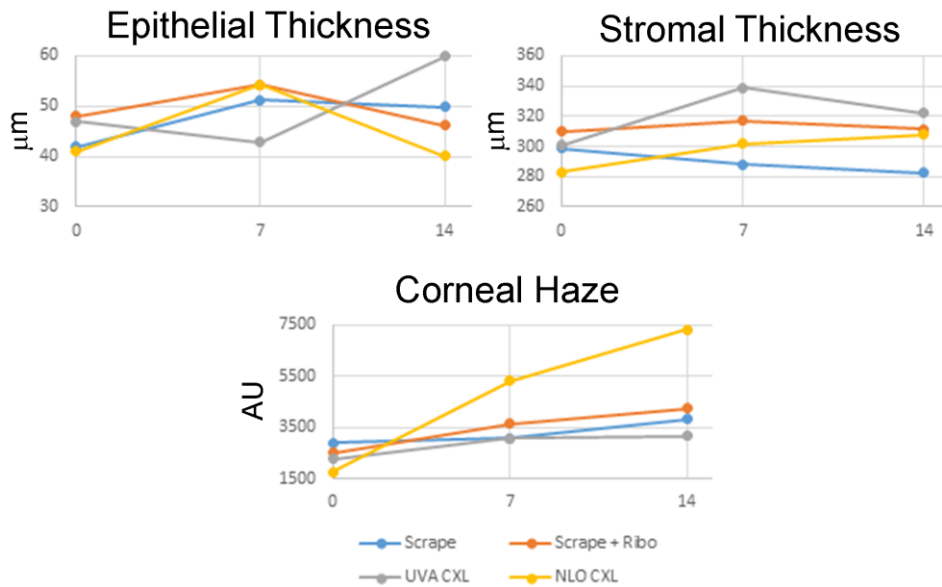


**Figure 19: CMTF Data of Initial In Vivo Study**

Epithelial thickness, stromal thickness, and haze measurements of various in vivo treatments over two weeks.

## Discussion

In vivo CMTF imaging showed high scattering at one and two weeks of treatment for all treatments, especially in the rabbit treated with NLO CXL at 900 mW. This indicates a cellular activity in the treatment zone lasting longer than the length of the study. Mechanical measurements using the indentation method previously described and CAF analysis were also attempted but results were highly variable, likely due to the extremely small sample size and the issues discussed in Chapter 2.

It should also be noted that this set of experiments was intended to be used as a means of streamlining our techniques for future in vivo experiments. For example, simple things such as how a rabbit needed to be positioned under the device, how to excise the corneal stroma quickly enough to perform mechanical testing before dehydration, or how to find the area of crosslinking post sacrifice were all issues unique to a first time experiment that greatly affected the results. More important than the actual results from this particular experiment were the questions it raised. As we analyzed the data and reviewed the literature it became clear that we needed more information on the general effects of collagen crosslinking in the corneal stroma.

# Chapter 4: Collagen Fiber Crimping Analysis

## Introduction

As previously stated, UVA CXL treatment has many known effects on corneal tissue, including a dose dependent cellular toxicity, corneal haze, collagen fiber thickening up to 12% within the crosslinked region, and possibly straightening of the collagen fibers.<sup>7, 12, 14-16, 22</sup> Keratocytes and endothelial cells are both at risk of damage, and cell death occurs within the crosslinked volume.<sup>22-26</sup> It has previously been observed that keratocyte repopulation begins around one month post crosslinking in rabbits,<sup>23-25</sup> with full repopulation at six weeks. Wollensak<sup>25</sup> and Kozobolis<sup>23</sup> both used light microscopy to observe keratocyte repopulation into the irradiated region. Wollensak reported full cellular repopulation by 6 weeks. Both reported a continuing presence of acellular areas and apoptotic changes such as apoptotic bodies, shrunken cell nuclei, and chromatin condensation at 4 weeks, especially around the periphery of irradiation. Kruger<sup>24</sup> also observed cellular repopulation by 6 weeks using a combination of confocal laser scanning microscopy and two photon excited fluorescence, but observed a lower cellular density than seen in controls.

In addition to observing wound healing after crosslinking treatment, many previous studies have focused on changes to the collagen fibers and/or lamellae post treatment, particularly the waviness or crimping of the fibers and/or lamellae. Various measurements of collagen crimp in the cornea or sclera have been made, including waviness, fiber orientation, or branching point density, and methods for obtaining these measurements include a wide range of imaging techniques, including computational models, light microscopy, MRI, x-ray scattering, and many more.<sup>24, 43-48</sup> In particular, SHG signals,

which are the result of frequency doubling of near infrared irradiation through noncentrosymmetric materials, have been useful for imaging corneal collagen lamellar structure.<sup>1, 24, 43-54</sup> This study is novel in that it examines the collagen crimp in specific regions of the cornea associated with enhanced collagen autofluorescence, a marker for collagen crosslinking.

The first objective of this study was to monitor in vivo changes after UVA CXL treatment. CMTF was used to monitor measurements of corneal thickness and haze during healing, and fluorescent staining was performed after sacrifice to observe cellular differences at one and three months post treatment. Another aim of this study was to measure degree of crimping in collagen after treatment. SHG imaging was used to detect a decrease in fiber crimping. Finally, CAF was measured at both time points with the intention of assessing the persistence of collagen crosslinking and precisely locating the region of crosslinking within each cornea.

## **Materials and Methods**

### *Animals:*

For this experiment two groups of four rabbits each, ages 3 to 9 months, were treated with standard UVA CXL in the right eye. All animals were treated according to the ARVO statement on the use of animals in vision research and experiments were approved by the IACUC of the University of California, Irvine. The first group consisted of 4 Dutch belted rabbits which were sacrificed one month after treatment. The second group consisted of 4 New Zealand albino rabbits sacrificed three months after treatment. In both cases the opposite eye of each animal was left untreated to be used as a control.

Prior to treatment, all rabbits were sedated as described in Chapter 3, with a subcutaneous injection of 30-50 mg/kg ketamine hydrochloride (Hospira, Irvine, CA) and 5-10 mg/kg xylazine (Akorn, Lake Forrest, IL), and images were taken of the right cornea using in vivo CMTF imaging to provide baseline measurements of epithelial and stromal thickness, and corneal haze.

### *Treatment:*

UVA CXL treatment was performed using a standard UVA CXL protocol.<sup>6, 7, 18</sup> Rabbits were initially sedated using ketamine/xylazine, with additional sedation as needed. Each animal then received a drop of topical ophthalmic 0.5% tetracaine hydrochloride (Alcon, Ft. Worth, TX) to prevent pain during treatment. Using a lid speculum to keep the eye open, the central 8 mm of the right cornea was marked with an 8 mm diameter trephine. The epithelium was then removed from this region by gently scraping the surface with a Tooke knife. Next sterile photosensitizing solution comprising of 0.1% riboflavin-5-phosphate (Sigma-Aldrich, St. Louis, MO) solution in phosphate buffered saline (PBS: pH 7.2) containing 20% high-fraction dextran, molecular weight 450-650 KDa (Sigma-Aldrich, St. Louis, MO) was applied to the stroma dropwise every two minutes for 30 minutes. Just as in experiments using ex vivo eyes, corneas were then exposed to 370 nm UVA light at 3mW/cm<sup>2</sup> for 30 minutes with continued application of riboflavin solution every 2 minutes. After treatment, each rabbit received a drop of 0.3% gentamycin sulfate (Allergan, Inc., Irvine, CA) in the treated eye. Each rabbit was treated with gentamycin eye drops three times daily for three days post treatment to prevent infection.

### *In Vivo CMTF Imaging:*

After treatment rabbits were monitored during healing using CMTF imaging to measure changes in epithelial thickness, stromal thickness, and corneal haze using techniques previously reported.<sup>40-42</sup> In addition to the intensity peaks correlated to natural structures such as the epithelium, an increased area of intensity, or haze, can easily be seen within the cross sections of treated eyes. Epithelial and stromal thickness were calculated as before, and a measure of haze was obtained by finding the area under the curve within the stroma.

CMTF measurements were taken pre-operatively and at 2, 4, 8, and 12 weeks. All rabbits were sacrificed following their last CMTF measurements at 4 weeks (4 rabbits) and 12 weeks (4 rabbits) using a 1 ml injection of Euthanasia III (Vedco, Inc. St. Joseph, MO) into the marginal ear vein.

### *CAF Imaging:*

Immediately after sacrifice eyes were perfusion fixed in situ at 20 mmHg using 2% paraformaldehyde (PFA, Mallinckrodt Baker, Inc., Phillipsburg, NJ) in PBS for 5 minutes to maintain the in vivo collagen structure. It has been previously shown that corneas fixed in this way do not exhibit any artifact as a result of the mechanical unloading of collagen fibers as the cornea is removed from the globe, or as a result of the fixation itself.<sup>52</sup> Corneas were then excised and left in PFA overnight at 4° C. The corneas were then sectioned and imaged as before.

Sections were imaged for CAF, as previously described.<sup>10, 31, 32</sup> Since CAF is known to be enhanced by induced crosslinking,<sup>10</sup> and to be correlated with increased

mechanical stiffness,<sup>31, 32</sup> it was used to locate the area of treatment and determine whether the stiffening effect had persisted over time. SHG images were then taken within the same sections, using two photon excitation at 820 nm, and collecting 390-465 nm, to observe the corneal collagen matrix, and to examine the crimping within the collagen structure. SHG imaging has often been used to study corneal collagen organization.<sup>1, 49-54</sup> Image stacks, 100-200  $\mu\text{m}$  deep and 427  $\mu\text{m}$  wide, were taken in varying areas of each section using a 40x objective (1.3 NA), so as to cover the entire epithelial to endothelial thickness in each image. Four SHG image stacks were taken per treated cornea, two in the central cornea, and two in the untreated periphery, outside of the region showing CAF. One SHG image stack was taken per control cornea, in the central region. Finally, sections were stained with phalloidin [1:100] and propidium iodide (0.001 mg/ml) to label extracellular f-actin and DNA respectively. Fluorescent imaging was performed on stained sections using an excitation of 488 nm and collecting 500-550 nm and 565-615 nm for phalloidin and propidium iodide respectively to observe cellular differences between samples.

### *Image Analysis:*

CAF was measured as described in Chapter 1 and 2.<sup>31, 32</sup> CAF was also used as a means of locating the treatment zone for SHG imaging. To quantify crimping of collagen, three planes within each SHG image stack were used for calculation. In each plane, the path of three fibers were traced across the entire width of the image using Metamorph (Metamorph; Molecular Devices) in both the anterior (region showing increased CAF) and posterior stroma. A value for collagen fiber crimping (CFC) was calculated as a ratio of

the length of the traced fiber to the length of a straight path in the same location. An example of this measurement is shown in Figure 20. These values were calculated for the central treated region and periphery of each treated cornea as well as the central region of each control cornea.

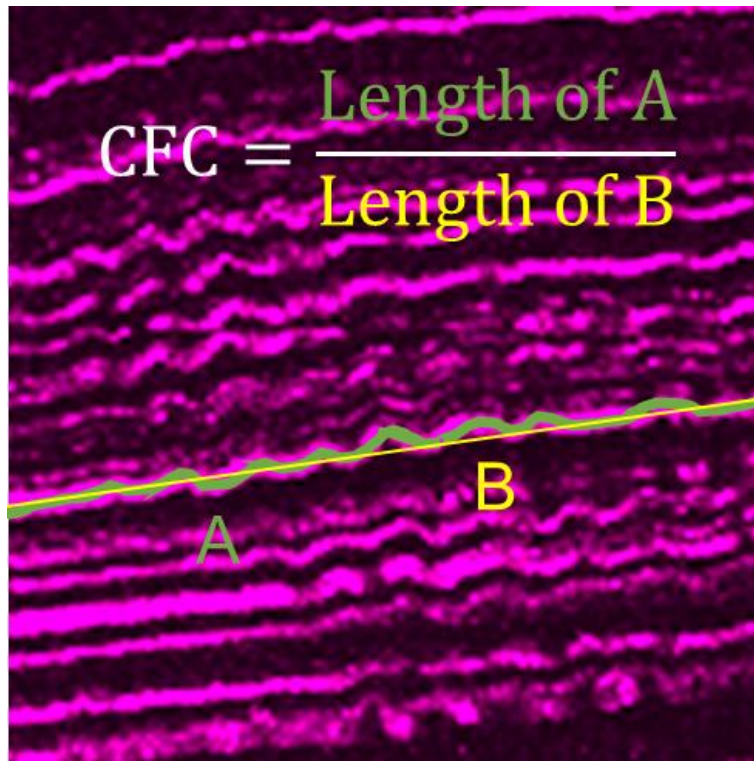


**Figure 20: Calculation of CFC**

CFC was calculated as the path length of a collagen fiber (A) divided by the length of a straight line through the same space (B). Reprinted/ adapted with permission from Experimental Eye Research.<sup>27</sup>

## Results

### *CMTF:*

Measurements of epithelial thickness, stromal thickness, and haze over time are graphed in Figure 21 and listed in Table 2. As shown in Figure 21A, measurements of epithelial thickness over time remained consistent, showing no significant differences ( $P > 0.6$ ) in either group. Stromal thickness (21B) however did show significant changes. By 3 months, in group 2, it had surpassed its original baseline thickness of  $301.5 \pm 4.9 \mu\text{m}$  to  $327.4 \pm 8.2 \mu\text{m}$ , a change of  $25.9 \mu\text{m}$ . While it was statistically significant, the increase was less than 10%, not likely clinically significant. In both groups haze (21C) increased for the first month following treatment, the most significant increase measured at 2 weeks post treatment with a 5.5 fold and 3.1 fold increase in groups 1 and 2 respectively. In both groups haze peaked at one month, with values of  $2277 \pm 272$  and  $2168 \pm 334.1$  in arbitrary units (AU). It then began to decrease in group 2 to a final three month value of  $1207 \pm 126.7$ . This was significantly decreased from the one month peak, and was no longer significantly increased from baseline. The CMTF cross sectional views shown in Figure 22 provide a visual representation of this change in haze over time.

As expected, examination of CMTF images also revealed an acellular zone in the anterior cornea. The increased intensity of the hazy region, shown in Figure 22, followed this acellular region.

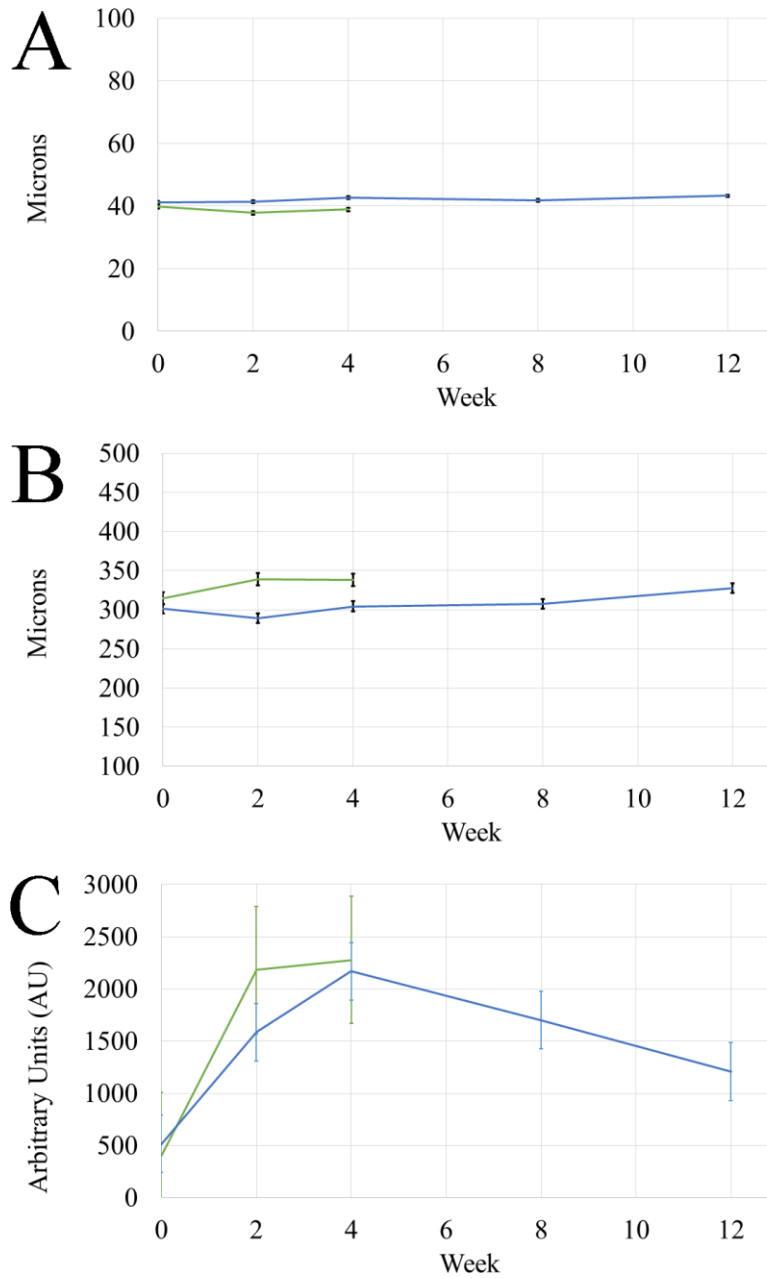


**Figure 21: In Vivo CMTF Measurements**

Changes in epithelial and stromal thickness for both groups were measured over time. Plots of these measurements are shown in A and B respectively, with week 0 referring to initial baseline measurements prior to treatment and all other time points referring to the number of weeks after treatment. Graph C shows the haze measured in arbitrary units at each time point. Reprinted/ adapted with permission from Experimental Eye Research.<sup>27</sup>

**Table 2: Corneal Thickness and Haze<sup>27</sup>**

Week	Epithelial Thickness		Stromal Thickness		Haze	
	1 Month	3 Month	1 Month	3 Month	1 Month	3 Month
<b>0</b>	39.9 ± 0.5	41.2 ± 1.4	314.5 ± 15	301.5 ± 4.9	399.5 ± 55.1	514.6 ± 75.7
<b>2</b>	37.8 ± 0.9	41.4 ± 1.9	338.8 ± 3.5	288.8 ± 9.1	*2180 ± 333	*1585 ± 236
<b>4</b>	38.9 ± 1.7	42.7 ± 0.9	337.9 ± 8.7	304.4 ± 8.6	*2277 ± 272	*2168 ± 334
<b>8</b>	NA	41.8 ± 0.6	NA	307.3 ± 6.9	NA	*1700 ± 254
<b>12</b>	NA	43.3 ± 0.6	NA	*327.4 ± 8.2	NA	1207 ± 127
*P<0.05 compared to Week 0						

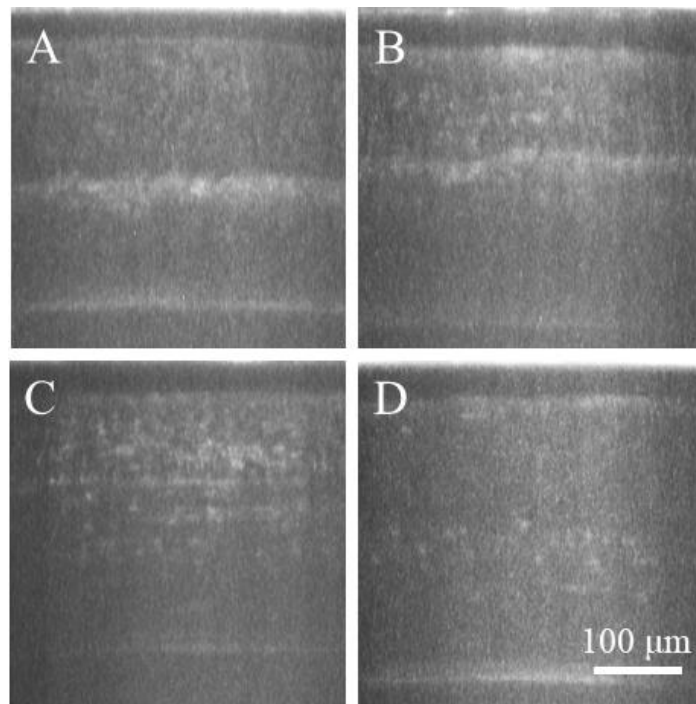


**Figure 22: Cross Sectional CMTF Images**

CMTF images showed haze at each week, corresponding to 2 (A), 4 (B), 8 (C), and 12 (D) weeks post treatment. Each image is a cross sectional projection of the through focus images taken at each time point. At the two week time point (A), most of the haze is concentrated to the area just below the treated region. Throughout recovery (B-D) haze spreads, peaking in intensity at one month (B), and then decreases. Reprinted/ adapted with permission from Experimental Eye Research.<sup>27</sup>

## CAF:

Representative CAF images from one and three months post CXL are shown in Figure 23. CAF averaged  $1267 \pm 181$  AU at one month and  $1224.2 \pm 158$  AU at three months in the two separate groups which was not significantly different. There was also no significant difference between the depths of crosslinking in either group, measuring  $42.4 \pm 3.4\%$  and  $47.7 \pm 7.6\%$  of the total thickness.

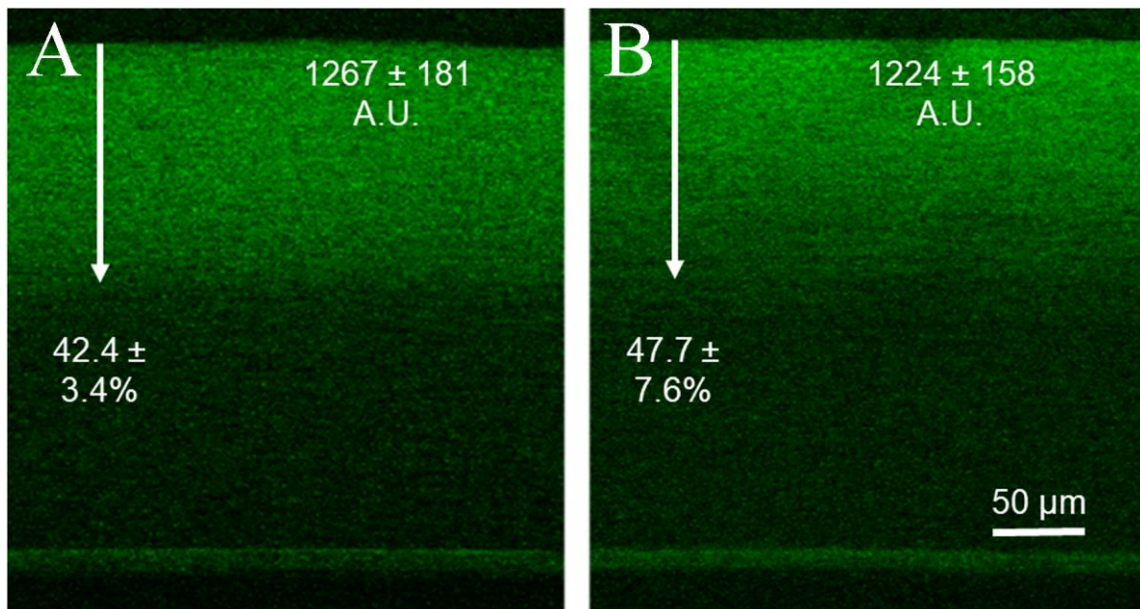


**Figure 23: CAF after 1 and 3 Months**

(A) A CAF image taken within the central region of a one month sample. The average intensity increase in these samples was  $1267 \pm 181$ . The depth of crosslinking, measured by depth of increased intensity and demonstrated with an arrow in the image, was found to be  $42.4 \pm 3.4\%$  of the total stromal thickness on average at one month. (B) The corresponding CAF image for the three month samples. CAF intensity and depth remained constant between the two time points with values of  $1224 \pm 158$  and  $47.7 \pm 7.6\%$  at three months. Reprinted/ adapted with permission from Experimental Eye Research.<sup>27</sup>

### *Collagen Crimping:*

Figure 24 shows representative images of each region used to measure crimp in both one (A and B) and three (C and D) month samples, and control (E and F). CFC values calculated for each region are shown in Table 3. At one month, the crosslinked region showed a significantly decreased measure of crimp compared to all other regions. In the anterior of the control sample (E), crimp measured  $1.017 \pm 0.004$ , that is, 1.7% longer than a straight path. When looking at the anterior of the central region of the one month treated cornea (A), crimp measured  $1.0067 \pm 0.0058$ , which is significantly straighter compared to control ( $P < 0.05$ ). In the periphery of treated eyes, outside of the region of CXL, crimping was  $1.017 \pm 0.0013$ , no different than the control (E and F). Also, no significant difference was detected between any values in the posterior stroma. Similarly, at three months, the anterior region of the CXL cornea was the only region with significantly lower crimp measurements, averaging  $1.009 \pm 0.0049$  (C), which was not significantly different from one month.

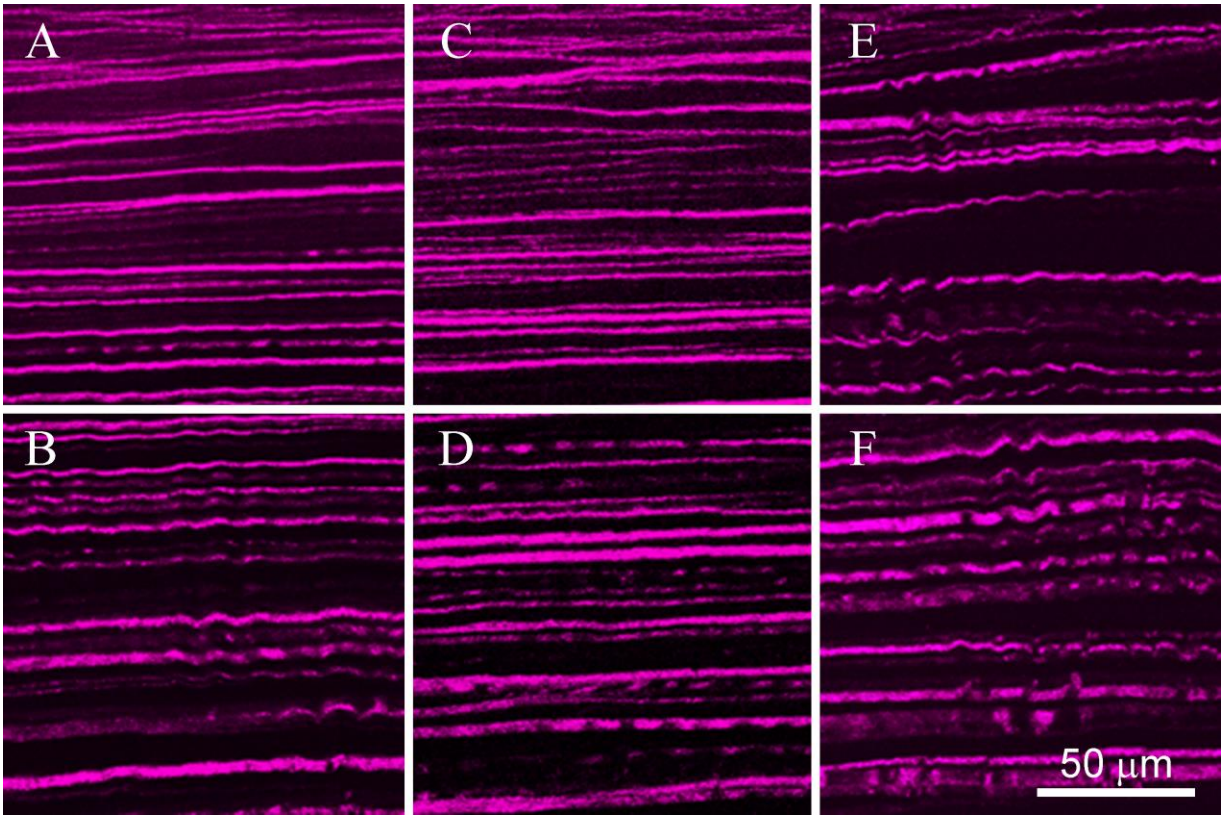


**Figure 24: SHG Images of Collagen Crimping**

Cross sectional SHG imaging revealed significantly straighter collagen fibers in the anterior of treated corneas at both one and three months (A and C respectively) when compared to their own posterior values (B and D) or control anterior or posterior values (E and F). Fibers were visibly wavier in all non-treated areas (B, D, E, and F). Reprinted/ adapted with permission from Experimental Eye Research.<sup>27</sup>

**Table 3: Collagen Fiber Crimp Data<sup>27</sup>**

Treatment	Time	Central		Peripheral	
		Anterior	Posterior	Anterior	Posterior
UVA CXL	1 Month	*1.007 ± 0.006	1.016 ± 0.004	1.017 ± 0.01	1.019 ± 0.07
	3 Month	*1.009 ± 0.005	1.022 ± 0.008	1.019 ± 0.06	1.019 ± 0.06
Control	1 Month	1.017 ± 0.04	1.022 ± 0.05	NA	NA
	3 Month	1.016 ± 0.06	1.024 ± 0.08	NA	NA

\*P<0.05 compared to corresponding posterior or control values

### *Cellular Repopulation:*

Although confocal images showed a significant reduction in haze from one to three months, staining with phalloidin and PI showed incomplete repopulation of cells into the acellular zone of the central cornea, seen in Figure 25A (1 month) and 25C (3 months). Images taken in the central cornea show almost no repopulation at either time point, indicated by the lack of keratocytes in the region of CAF, shown in blue. Additionally, the depth of the acellular region is not significantly different than the depth of CAF at both time points,  $40.5 \pm 4.1\%$  versus  $42.4 \pm 3.4\%$  at one month and  $43.7 \pm 11.3\%$  versus  $47.7 \pm 7.6\%$  at three. This is also in agreement with CMTF images taken within the treatment region, which show no cells anterior to the region of haze at all time points. In the periphery, however, cellular migration into the area of CXL was observed at one month, which appeared greater at three months, Figure 25B and 25D.

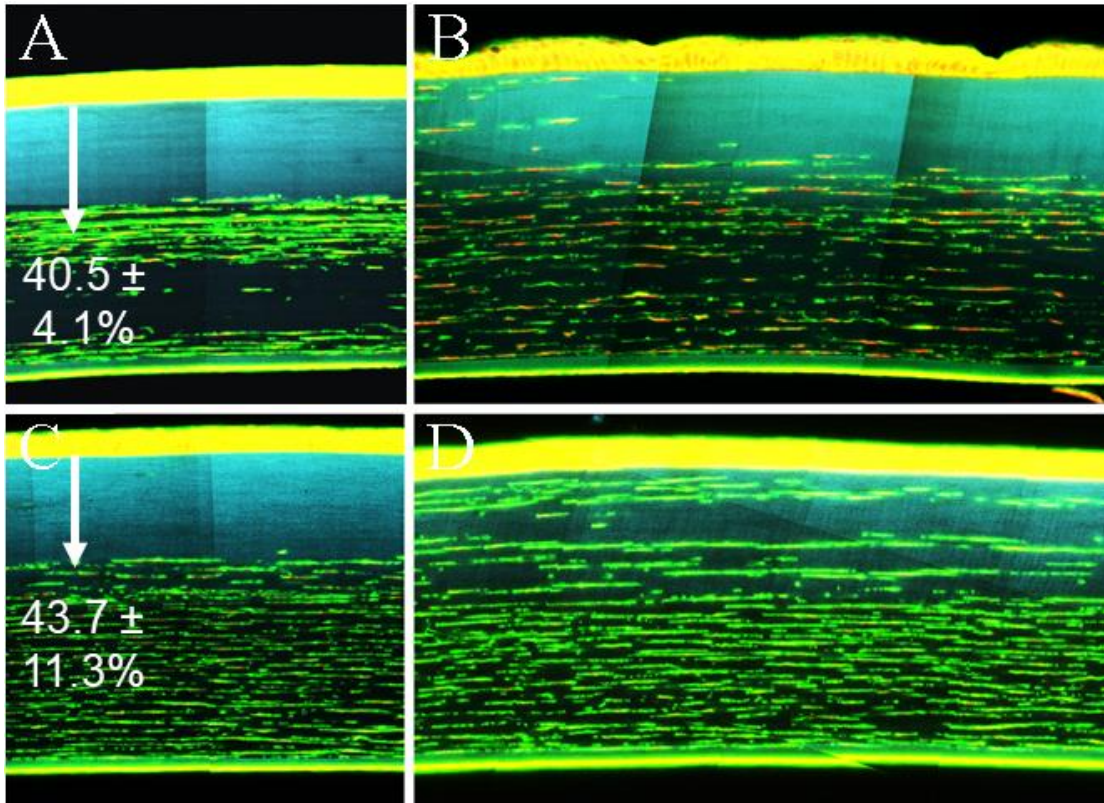


**Figure 25: Cellular Staining after Crosslinking**

(A and B) Show samples from the central CXL region and the edge of the CXL region bordering the periphery from one month samples. (C and D) Show corresponding images from three month samples. Staining with Phalloidin (green; 1:100) and Propidium Iodide (red; 0.01 mg/ml) showed little cellular repopulation into the central CXL region, shown with blue CAF, at either time point. Images from the periphery show migrating cells into the CXL region. The depth of the acellular zone in the central cornea is indicated by arrows and measured as a percent of the stromal thickness. This corresponds to the measured depth of CAF. Also, in two of the four one month samples, a second deeper acellular region was noted, pictured in A. Reprinted/ adapted with permission from Experimental Eye Research.<sup>27</sup>

These images also yielded an unexpected result. As shown in Figure 25A, one month samples appeared to have a loss of keratocytes in the posterior, un-crosslinked region. In two of the four samples this area was almost entirely acellular. Three month samples showed a more uniform cellular distribution below the crosslinked region, Figure 25C.

## Discussion

Little change was detected in epithelial or stromal thickness, but a large change was detected in corneal haze during healing. This is in agreement with the temporary haze others have observed clinically.<sup>13</sup> Stromal thickness did show a slight but steady increase over time, which was only significantly different after the full three months. This was likely not a result of the crosslinking procedure itself, but of the natural aging of the animal. It has been shown that the central thickness of rabbit corneas increases steadily with increasing age at a rate consistent to that seen in this study, about 25  $\mu\text{m}$  in a three month period.<sup>55</sup>

Fluorescent cellular staining on corneal sections provided a better view of the cellular differences between one and three month samples than was possible using CMTF. Contrary to previous reports, which indicated cellular repopulation after 4-6 weeks of recovery in rabbits,<sup>23-25</sup> cellular repopulation was only observed in the peripheral cornea, around the edges of the CXL area. This was shown both visually in the images and quantitatively when CAF depth was compared to cell depth, and no difference was found. Images taken at the edge of the treated region did show more cells which overlapped the blue CAF at one month (25B), and even more at three months (25D). This indicates that cells are migrating in from the periphery, consistent with previous reports.<sup>23,</sup><sup>25</sup> Contrary to these reports, however, cellular repopulation was not fully completed after three months. The current study is more consistent with the results from Kruger,<sup>24</sup> who reported cellular migration beginning as early as 3 days and repopulation at 6 weeks which still lacked the full cellular density of controls. The authors of that report cited the youth of the rabbits used as an explanation for earlier repopulation than expected. Also

observed in the stained sections was a region of fewer or no cells at one month in the posterior central cornea, outside the area of CAF (25A). This finding was not detected by the in vivo CMTF imaging, possibly because of the lower resolution of that technique. This is in agreement with literature<sup>23</sup>

It should also be noted that no change in CAF was observed between 1 month and 3 months after crosslinking. Previous studies have linked changes in CAF to changes in stiffening using both mechanical indentation testing and enzymatic digestion.<sup>10, 31, 32</sup> Therefore the finding that CAF is not changed over time suggests that the stiffening effect may also persist for at least three months. This is in agreement with mechanical studies, which have also shown a persistence in the stiffening effect, and with clinical studies which show a lasting visual improvement.<sup>11, 13</sup>

Lastly, many groups have studied the changes in corneal collagen and corneal shape following UVA CXL with clinical studies showing a significant reduction in corneal curvature.<sup>7, 12-17</sup> This study identified a significant reduction of collagen crimping following UVA CXL in vivo, a change which persisted over time, and was present only within the treatment region as identified by CAF. There are at least three plausible explanations for this observation. 1) Reduction in collagen crimp could be due to the resistance of relaxation of crosslinked fibers or an artifact of fixation, 2) Straightening of fibers is due to corneal edema, or 3) Collagen straightening is due to collagen fiber shortening.

The first explanation of our collagen crimping observations assumes that the treated area, being mechanically stiffer than surrounding tissue, does not relax in the same manner when the cornea is excised. This would cause skewed crimping comparisons. The corneas in this study, however, were fixed under pressure to avoid this

artifact, which has previously been shown to be effective.<sup>52</sup> Also, it is worth noting that crimping due to any other fixation artifact would likely have affected the whole tissue, not just the periphery.

The second explanation assumes that a swollen cornea should have straighter fibers. There are several observations indicating that this may not be the case. For example, clinical results show a wide range of both increasing and decreasing corneal thicknesses after treatment, while still showing a trend of reduced corneal curvature.<sup>14</sup> This suggests that the cause of fiber straightening is more complex than just edema. Moreover, since the corneal thickening seen in this study did not occur immediately after treatment, but gradually over time and was consistent with observations of age related changes in corneal thickness of rabbits in the literature,<sup>55</sup> we believe that the increase in thickness observed in this study was not edema caused by treatment but was instead a natural aging process. More specifically, if the increase in thickness was due to edema that caused decreased collagen fiber crimping, then we should have observed significantly less crimping at 3 months compared to 1 month after crosslinking, which was not the case. It has also been shown that when swelling does occur in the corneal stroma, it happens predominantly in the posterior, leaving the anterior structure unchanged.<sup>56</sup> Swelling was also noted by Muller et al. to cause increased waviness of the collagen lamellae, which would result in increased crimp, not decreased crimp. Finally, there is also evidence in the literature showing that collagen crosslinking reduces the swelling pressure within the treatment region, making it unlikely that crosslinking induces edema in the region of treatment.<sup>57</sup>

The final explanation is that collagen straightening, and corneal flattening could be due to fiber shortening. If fibers are shorter after crosslinking, it would be logical that they would also be straighter. If the arc length across the cornea is the same or reduced after the procedure, and the fiber length were to remain constant, then a region of straightened fibers would have to result in increased crimp outside of the treatment region. In other words, the fiber would have to go somewhere. This study showed no change in crimp in any of the surrounding regions. This observation, combined with the evidence listed against the first two explanations leads us to believe this is the most plausible of the three explanations. Furthermore, other studies have observed changes in the extracellular matrix, including increased collagen fibril diameter and decreased interfibrillar spacing, all of which could be associated with collagen fibril shortening.<sup>24, 53, 58</sup> It is unlikely that all these changes are independent of one another, and therefore it is likely that they all play some role, directly or indirectly, to affect corneal curvature.

## Chapter 5: Amplified NLO CXL

### Introduction

As stated in the Issues section of Chapter 2, a major hurdle of our initial NLO CXL system that needed to be overcome was the issue of total power exceeding the ANSI limit of 46.1 mW. These previous studies used a high repetition rate (80 MHz) low pulse energy (10 nJ) laser oscillator to effect crosslinking, resulting in the high average power (>800 mW). We knew from our previous work in Chapter 1 that there existed a linear relationship between pixel dwell time (or total energy deposition), and CAF intensity.<sup>31</sup> This indicates that increased pulse energy may enhance the crosslinking effect. For this reason we hypothesized that there may exist some optimal pulse energy, higher than what was used in our earlier study, which allows for more efficient excitation of riboflavin. If the efficiency of the riboflavin excitation is optimized, it may then allow for a drop in the overall laser power to below ANSI limits. The 80 MHz system used in those early studies, however, was limited to pulse energies on the order of 10 nJ. By switching to a laser with regeneratively amplified fs pulses, the effects of higher pulse energies could be studied.

This study explored using regeneratively amplified fs laser pulses, with  $\mu\text{J}$  pulse energy, at low repetition rates (kHz) to precisely crosslink corneal collagen while remaining under the ANSI limit of 46.1 mW. A custom non-collinear optical parametric amplifier (NOPA) was designed and built to deliver 760 nm, amplified fs laser pulses at repetition rates of 50-100 kHz. Amplified nonlinear optical corneal collagen crosslinking (amplified NLO CXL) was performed in ex vivo rabbit eyes after which CAF and mechanical stiffness measurements were performed. Crosslinking experiments were also

carried out in live rabbits and topography was measured to assess refractive outcomes of amplified NLO CXL in vivo.

## **Materials and Methods**

### *Proof of Concept:*

Prior to building a custom amplified NLO CXL system, the question of whether NLO CXL was even possible using amplified fs pulses was investigated by examining CAF within ex vivo rabbit eyes treated using a commercially available regeneratively amplified titanium sapphire fs laser (Legend-F, Coherent Inc., Santa Clara, CA) and optical parametric amplifier (Opera, Coherent Inc., Santa Clara CA) coupled to our delivery optics. The 5 kHz, 130 fs, 800 nm laser output from the Legend was directed into the Opera OPA, generating 1520 nm pulses, which were then frequency doubled in a BBO crystal to produce a 760 nm pulses with 1  $\mu$ J pulse energy. Using this repetition rate it was possible to put 3  $\mu$ m between each individual pulse, for single pulse crosslinking. CAF was examined within both vibratome sections and en face within the whole sample. All tissue preparation and imaging were performed using previously reported techniques, and were identical to methods used in the remainder of this study.<sup>27, 31, 32</sup> Objectively high CAF Intensity was observed after just a single, 1  $\mu$ J pulse of amplified NLO CXL with average power of only 5 mW (A huge reduction in total required energy). Presence of CAF within these samples, Figure 26, was used as justification for building a more stable system with a higher repetition rate, enabling crosslinking at faster scan speeds.

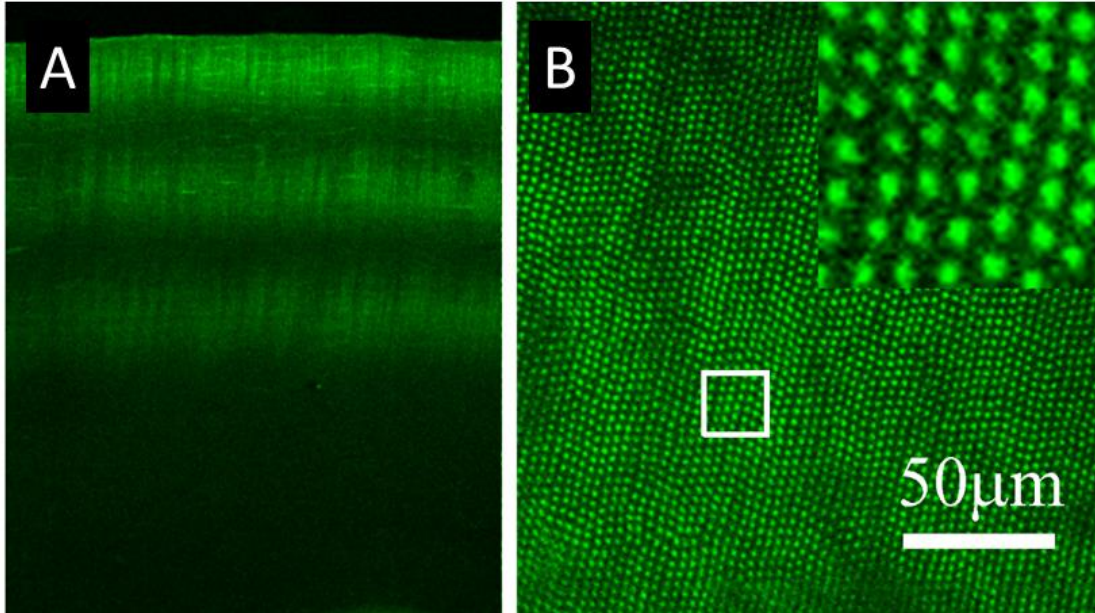


**Figure 26: CAF of Single Spot Amplified NLO CXL**

The image shown in (A) demonstrates the CAF within a vibratome section of a cornea treated with three separate layers of single spot amplified NLO CXL. (B) shows the en face view of a cornea treated in the same way. A grid of CAF spots can clearly be seen within the sample.

### *Amplified Femtosecond Laser and Delivery:*

Though commercially available fs oscillators are broadly tunable and can readily deliver 760 nm fs laser pulses, commercial turnkey amplified fs laser systems are not available at this wavelength. However, photons of different wavelengths can be generated from an fs laser source using nonlinear processes in an optical parametric amplifier (OPA). In this study, we used a commercially available amplified fs laser operating at 1030 nm, 100 kHz, 318 fs pulse duration, and 4 W average power as the laser source for a lab built NOPA (One Five Origami, NKT Photonics, Blokken 84, 3460 Birkerød, Denmark). The NOPA generated  $\mu\text{J}$  760 nm fs pulses which were then aligned into the beam delivery/scanning device from our previous study<sup>32</sup> and then into the eye. An

overview of the entire system is presented in Figure 27. In general, a NOPA is a device capable of converting a pump photon of a specific wavelength into two photons of longer wavelengths, termed signal and idler. The wavelengths of the signal and idler can be continuously tuned as long as the requirement of energy conservation is met. The NOPA built for this study contains three stages: 1) Supercontinuum generation 2) Formation of the pump beam 3) Parametric conversion.

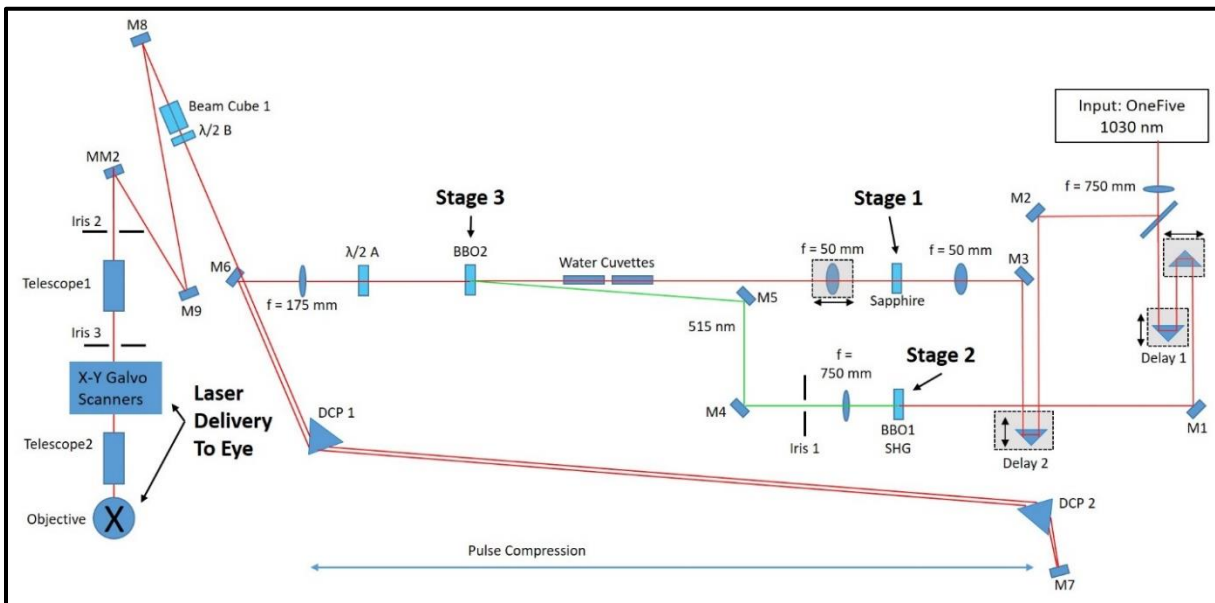


**Figure 27: Custom NOPA Schematic**

Schematic showing the components of the amplified NLO CXL device. The device consists of three main elements: 1) the laser source (OneFive regeneratively amplified FS laser). 2) Non-collinear optical parametric amplifier (NOPA) consisting of three stages (supercontinuum generation, frequency doubled pump beam generation, and parametric conversion). 3) Laser delivery system. Within the whole diagram, M indicates a mirror, and f indicates a lens of specified focal length.

### *Stage 1: Supercontinuum Generation*

Approximately 10% of the output of the 1030 nm laser source, is picked off by a beam splitter and focused onto a 200  $\mu\text{m}$  thick sapphire plate. Acting as a nonlinear medium, this spectrally broadens the original laser pulse via self-phase modulation creating supercontinuum radiation that appears like white light to the eye. Centered at 1030 nm, the supercontinuum radiation contains spectral components from 500 nm to 1500 nm. The output is well-formed and smoothly varying making it a suitable source to serve as the “seed” pulse for the NOPA. The white light is passed through two water cuvettes, adding group velocity dispersion to the supercontinuum, and ultimately reducing the bandwidth of the 760 nm NOPA output to 12 nm.

### *Stage 2: Pump Formation*

The remaining 1030 nm source beam is sent to a 2 mm thick beta barium borate (BBO) crystal for frequency doubling. The 2 mm BBO is responsible for converting the source from 1030 to 515 nm which can then be used to generate the two longer wavelength photons in the visible. BBO is used due to its large second order susceptibility,  $\chi^{(2)}$ , as well as its high damage threshold.

### *Stage 3: Parametric Conversion*

After frequency doubling in Stage 2, the 515 nm radiation is sent to a second 400  $\mu\text{m}$  thick BBO crystal, for parametric conversion. After passing through the second BBO crystal the 515 nm light produces a parametric ring of visible radiation. As the crystal angle is varied, color separation can be observed within the ring. The proper crystal angle

is determined by finding the angle that minimizes color separation. Once this angle is found, the supercontinuum seed from Stage 1 is spatially overlapped with the 515 nm pump in the second BBO crystal, and directionally overlapped with the parametric ring. After this is accomplished, the translation stage shown in Figure 27 is adjusted to ensure proper timing between the seed pulse and the 515 nm pump pulse. When both the seed and pump pulses are aligned spatially, directionally, and temporally, the parametric ring of radiation collapses into a beam which takes on the properties of the original pump beam. Owing to the fact that the supercontinuum seed is chirped, wavelength tuning can be accomplished by altering the timing of the seed relative to the pump pulse by adjusting delay 2 (Figure 27). For this study the center wavelength of the NOPA was adjusted to 760 nm with a FWHM bandwidth of 12 nm, as measured by a spectrometer (Thorlabs, Newton, NJ, USA). The pulse duration of the newly formed 760 nm beam was measured using a lab built auto-correlator and found to be ~700 fs. The beam is then passed twice through an SF10 ultrafast laser dispersion compensation prism (DCP in Figure 27) pair, which has the effect of compressing the pulse and thus controlling pulse duration. After compression the pulse duration was measured to be ~400 fs.

### *Laser Delivery*

Upon leaving the pulse compressor, the beam passes through a half wave plate ( $\lambda/2$  in Figure 27) and polarizing beam cube which function as a continuously variable beam attenuator. The rest of the beam delivery optics are identical to those used in our previous study.<sup>32</sup> The effective NA of the delivery system was found to be 0.12 for this study.

## *Amplified NLO CXL in the Ex Vivo Rabbit Cornea:*

Initial studies were performed in ex vivo rabbit eyes to first determine the feasibility of crosslinking using amplified fs pulses, and then to determine the amount of amplified fs laser energy deposition needed to achieve corneal crosslinking at levels equal to standard UVA CXL. The amount of energy deposition was controlled by varying the scan speed of the laser beam and thus the amount of laser pulses per unit area along the scan line. As in previous chapters, CAF was used as a metric to assess the degree of collagen crosslinking.<sup>29, 31, 32, 59-61</sup> CAF was compared against our previously published CAF data using standard UVA CXL in Chapter 4.<sup>27</sup> After a suitable energy was determined, we performed mechanical testing to determine the effect of amplified NLO CXL on tissue stiffness.

### *Scan Speed vs CAF*

A total of 29 ex vivo rabbit eyes were shipped overnight on ice (Pel-Freez, Rogers, AK) and experiments were performed the same day as delivery. The eyes were prepared for treatment with epithelial removal and 0.5% riboflavin soaking as in all other studies and described in Chapter 1. Amplified NLO CXL was then performed in the central 4 mm of the cornea. Treatment groups were defined by the scan speed of the laser beam, ranging from 5 mm/s to 100 mm/s. The beam was scanned in a raster pattern as described previously with a line separation of 5  $\mu\text{m}$  to shorten the scanning time required for this portion of the study.<sup>31, 32</sup> The pulse energy and average power were set to 0.3  $\mu\text{J}$  and 30 mW, respectively at 100 kHz pulse repetition frequency, well beneath the ANSI limit of 46.1 mW. The parameters for each treatment group as well as each group size

are outlined in Table 4. Each group had at least 3 eyes (n=3). The treatment times reported in this table were calculated for line separations of both 2  $\mu\text{m}$  and 5  $\mu\text{m}$ , since the 5  $\mu\text{m}$  separation used for CAF evaluation was later reduced to 2  $\mu\text{m}$  for mechanical measurements and in vivo treatments. The values for standard UVA CXL are provided for reference. After treatment, corneas were prepared for CAF measurements.

**Table 4: Scan Speed and Total Energy**

<b>Scan Speed (mm/s)</b>	<b>Group Size (n)</b>	<b>5 <math>\mu\text{m}</math> Treatment Duration (min)*</b>	<b>2 <math>\mu\text{m}</math> Treatment Duration (min)*</b>	<b>Total Energy (J)</b>
<b>100</b>	3	0.53	1.33	2.4
<b>80</b>	3	0.67	1.67	3.0
<b>60</b>	3	0.89	2.22	4.0
<b>40</b>	3	1.33	3.33	6.0
<b>30</b>	4	1.64	4.11	7.4
<b>20</b>	6	2.66	6.66	12.0
<b>10</b>	3	4.93	12.33	22.2
<b>5</b>	4	9.86	24.66	44.4
<b>UVA CXL</b>	NA	30	30	5.4
*Treatment time associated with a line separation of 2 or 5 $\mu\text{m}$ respectively				

CAF was measured per the protocol in our previous studies taking care to faithfully replicate the measurements, via laser power and microscope settings, to allow for reliable comparison between disparate time points.<sup>27, 31, 32</sup> Briefly, after amplified NLO CXL, corneas were excised from the globe and fixed overnight in 2% paraformaldehyde (PFA, Mallinckrodit Baker, Inc., Phillipsburg, NJ) in PBS at 4° C. Sections were then imaged for blue CAF with 760 nm excitation and 400-450 nm emission.

The images were exported to Metamorph image analysis software (Metamorph; Molecular Devices) and three 100 x 100 pixel areas within both the central anterior crosslinked region and the background region were identified. The average intensities within both regions were then subtracted. To compensate for the fact that line separation was not continuous in the NLO CXL treatment, resulting in dark areas between the scan lines (Figure 28) that would make the CAF data non comparable to previous UVA CXL CAF data, a percentage of crosslinked area was calculated from the NLO CXL samples using the FWHM values of a line scan inserted across NLO CXL CAF images. This percentage was used as a multiplication factor to convert previously reported UVA CXL CAF data from Chapter 4.<sup>27</sup>

#### *Corneal Stiffness Measurements*

Based on the results yielded from scan speed experiments, a speed of 20 mm/s was chosen for the stiffness experiments as this speed resulted in CAF comparable to that of UVA CXL and still had reasonable procedure time when the line separation was reduced back to 2  $\mu\text{m}$ . The total crosslinking time for this speed was approximately 6.66 min (Table 4). Mechanical measurements were conducted on corneas that underwent amplified NLO CXL (7) as well as control eyes (7). Three NLO CXL eyes were excluded because CAF analysis revealed the treatment region was outside the measured area. Two control eyes were excluded because their mechanical measurements were more than two standard deviations above the mean, indicating they were either old corneas, or had become dehydrated during testing. The same method presented in Chapter 2 was used to measure mechanical stiffness, and elasticity values was calculated based on the

peak force value of the 10<sup>th</sup> cycle using the equations, Eq (4), outlined by Hayes et al.<sup>32</sup>,

35, 36

### *In Vivo Amplified NLO CXL:*

A total of 14 New Zealand albino rabbits were used in this study. They were divided into two groups, 5 sacrificed 2 weeks after treatment and 9 after 2 months. All animals were treated according to the ARVO statement on the use of animals in vision research and experiments were approved by the IACUC of the University of California, Irvine. The right eye of each rabbit underwent amplified NLO CXL while the left eye served as a control. Both eyes of the short term group (2 week) were examined using in vivo CMTF imaging to study cellular activity just prior to sacrifice, and to measure the corneal thickness and scattering within the stroma after treatment.<sup>27</sup>

For the long term group the corneal topography was measured in both right and left eyes using an Orbscan Ilz (Bausch and Lomb, Rochester, New York) 1 week prior to treatment (baseline) and 1, 2, 4, and 8 weeks post treatment. Topography measurements were performed by an ophthalmologist with previous experience in topography measurements in the rabbit. Before all CMTF or topography procedures, animals were anesthetized with a ketamine/xylazine mixture following the established protocol discussed previously. The effect of the procedure was measured by calculating the difference in refractive power between the right and left eye at each time point ( $\Delta D=R-L$ ).

For amplified NLO CXL, sedated animals received a drop of topical ophthalmic 0.5% tetracaine hydrochloride (Alcon, Ft. Worth, TX) to prevent pain before removal of the central 8 mm of epithelium using a Tooke knife. The corneas were then imbibed with

0.5% riboflavin solution using the previously discussed protocol in Chapters 3 and 4. Each right eye then underwent amplified NLO CXL in the central 4 mm with a line separation of 2  $\mu\text{m}$  using a pulse energy and average power of 0.3  $\mu\text{J}$  and 30 mW at a laser scan speed of 20 mm/s. After treatment the rabbits received a subcutaneous 1 ml injection of buprenorphine hydrochloride (Reckitt Benckiser Healthcare Ltd., UK) for pain. For three days following the procedure each rabbit received an antibiotic eye drop, 0.3% gentamicin sulfate (Allergan, Inc., Irvine, CA), 3 times daily in the treated eye to prevent infection. After 8 weeks post treatment, animals were sacrificed via an intravenous 1 ml injection of Euthanasia III (Vedco, Inc. St. Joseph, MO) into the marginal ear vein after the last topography measurements. Immediately after sacrifice corneas were fixed in situ under 20 mmHg pressure via perfusion of 2% PFA to maintain the in vivo collagen structure, as described in previous studies.<sup>27</sup> The corneas were then excised and prepared for CAF measurements, in the same manner as described above for ex vivo eyes, to confirm the presence of crosslinking.

## Results

### *Ex Vivo Amplified NLO CXL:*

#### *Scan Speed vs CAF Intensity*

Example CAF images used for measurements are shown in Figure 28. The measured CAF intensities corresponding to each treatment speed are graphed in Figure 29. CAF intensity scaled downward logarithmically with increasing scan speed and fit to the equation  $y = -375.1\ln(x)+1806.6$  with an  $R^2 = 0.9814$ . Using the FWHM values from a line scan perpendicular through the crosslinked area of NLO CXL CAF images the

percentage of crosslinked area was measured to be 61.4%. Using Zipfel's equations (Eq 1-3), a comparable value of 58% was calculated.<sup>30</sup> UVA CXL CAF values reported in a previous study<sup>27</sup> (Chapter 4) were converted to  $777.9 \pm 111.1$  using this percentage to compensate for the spacing between scan lines in NLO CXL CAF images. Using this value, amplified NLO CXL reached a comparable CAF intensity to UVA CXL at a speed of 15.5 mm/s.

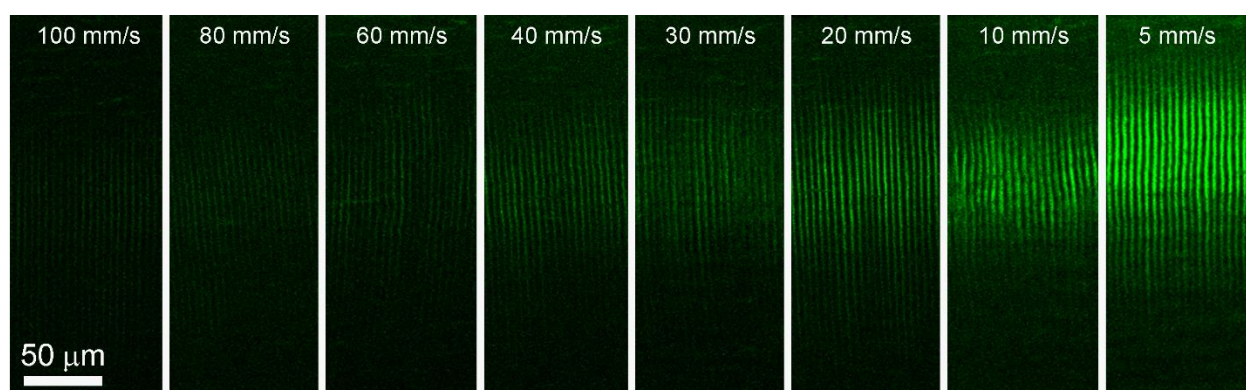


**Figure 28: Amplified NLO CXL Induced CAF vs Speed**

Example CAF images taken of ex vivo eyes treated with scanning speeds between 5-100 mm/s.

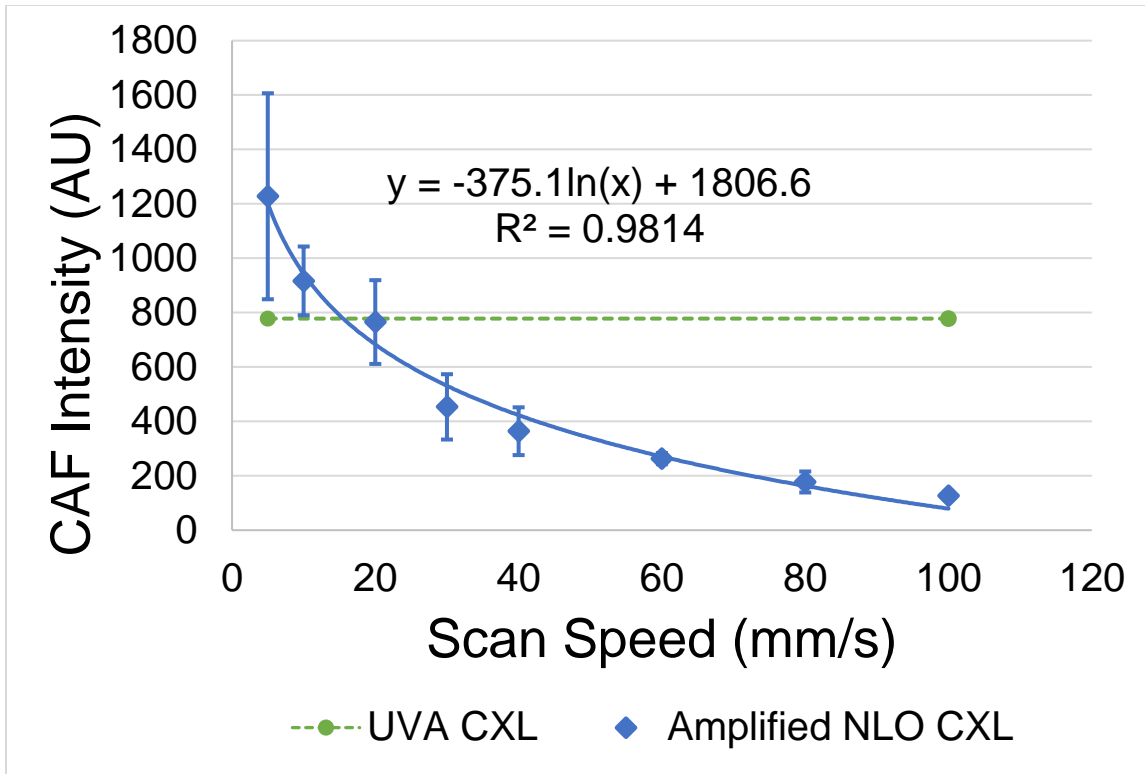


**Figure 29: CAF Intensity vs Scanning Speed**

CAF intensity of amplified NLO CXL treated eyes plotted with respect to increasing scanning speed, and compared to CAF of previously reported UVA CXL data.<sup>27</sup> The data fit the line  $y = -375.1\ln(x) + 1806.6$  with an  $R^2$  value of 0.9814, and intersected the UVA CXL CAF line at a speed of 15.5 mm/s.

### Corneal Stiffness

The elasticity values of corneas treated using amplified NLO CXL were measured to be  $84.3 \pm 5.9$  KPa (n=4) using the indentation method described, 1.62 times larger than control values measured to be  $52.2 \pm 8.6$  KPa (n=5). After statistical analysis this difference was found to be statistically significant. A comparison of these two values is provided in the graph in Figure 30.

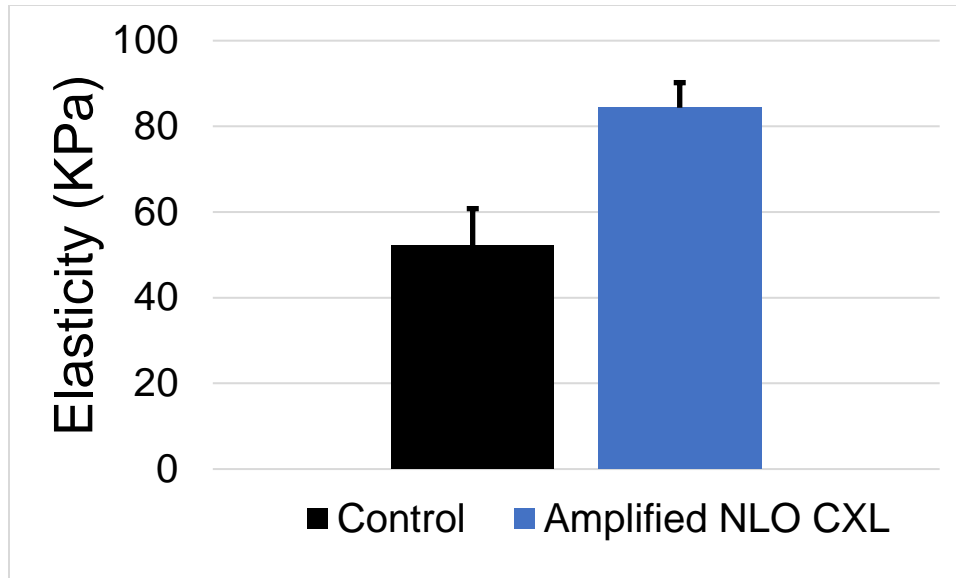


**Figure 30: Corneal Elasticity after Amplified NLO CXL**

Amplified NLO CXL (n=4) produced a 1.62 fold statistically significant increase in corneal elasticity compared to control corneas (n=5) (P<0.05).

### *In Vivo Amplified NLO CXL:*

Clinical observation of the corneas 48 hours after treatment revealed very little irritation of the tissue. No significant redness, swelling, or visible haze was observed, as can be seen in Figure 31A. 31B Shows CAF taken within a vibratome section after 2 weeks of healing. A consistent 110  $\mu\text{m}$  thick band of CAF can be seen 90  $\mu\text{m}$  below the surface of the epithelium. 31C and D show a cross-sectional CMTF image and a 178  $\mu\text{m}$  deep plane image within a cornea at 2 weeks. The scattering seen in C, and the spindle shaped cell bodies seen in D indicate cellular migration within the treated region at 2 weeks. CMTF imaging within the short term group also revealed a significantly thicker epithelium ( $42.4 \pm 1.5 \mu\text{m}$  vs  $36.1 \pm 1.8 \mu\text{m}$ ), an un-changed stromal thickness ( $315.6 \pm 23.7 \mu\text{m}$  vs  $310.6 \pm 19.2 \mu\text{m}$ ), and significantly increased haze ( $3148.1 \pm 622$  vs  $1303.1 \pm 527$ ) in treated eye compared to control.

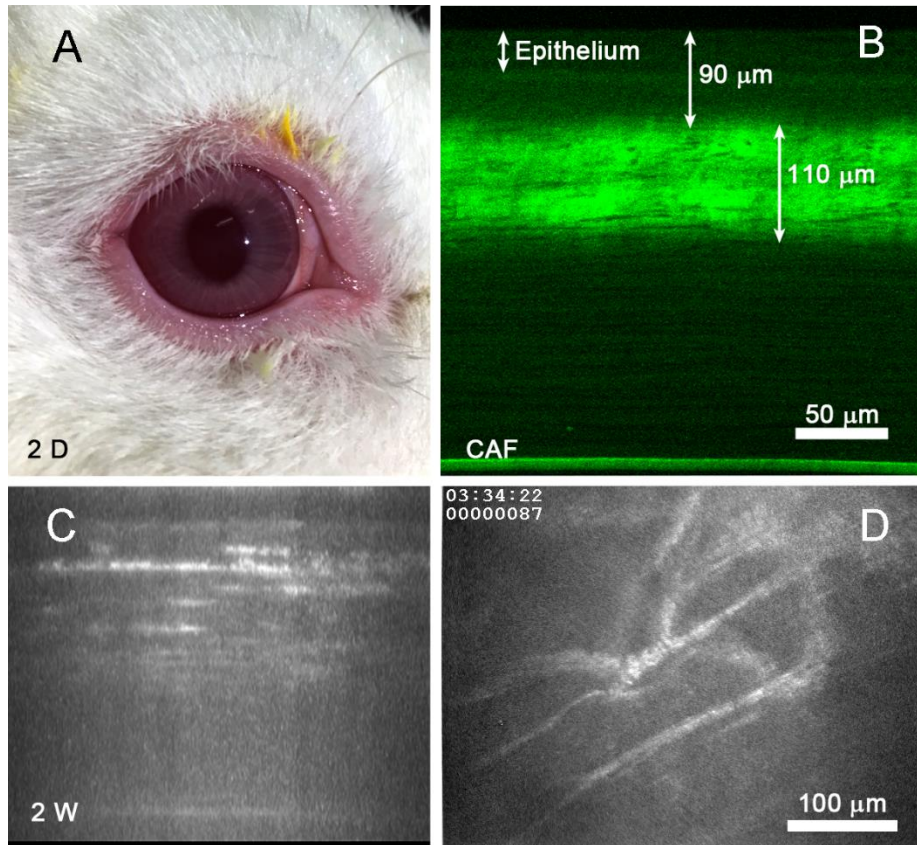


**Figure 31: Short Term Amplified NLO CXL**

The image in (A) is a clinical image of the cornea 48 hours after treatment, showing very little irritation. (B) is a representative CAF image showing a consistent region of CAF and an intact, regrown epithelium. (C) is a representative cross-sectional reconstruction of a CMTF stack taken at 2 weeks. (D) is a single plane CMTF image, 178  $\mu\text{m}$  deep, showing spindle shaped cellular structures within the treatment region.

In the long term group corneal flattening was measured as the diopter difference ( $\Delta D$ ) between the right and left eye (R-L) of each rabbit prior to treatment and at the intervals listed previously. For this reason, a negative value indicates flattening of the treated eye. Measurements of three rabbits were excluded because CAF could not be detected in the treated eye after sacrifice. Our previous studies have shown that CAF is

unchanged even after 3 months of healing,<sup>27</sup> so the lack of any CAF was considered indicative of a lack of CXL. The average  $\Delta D$  from the 7 remaining rabbits are graphed in Figure 32, and listed individually in Table 5. All time points showed significant flattening compared to baseline.

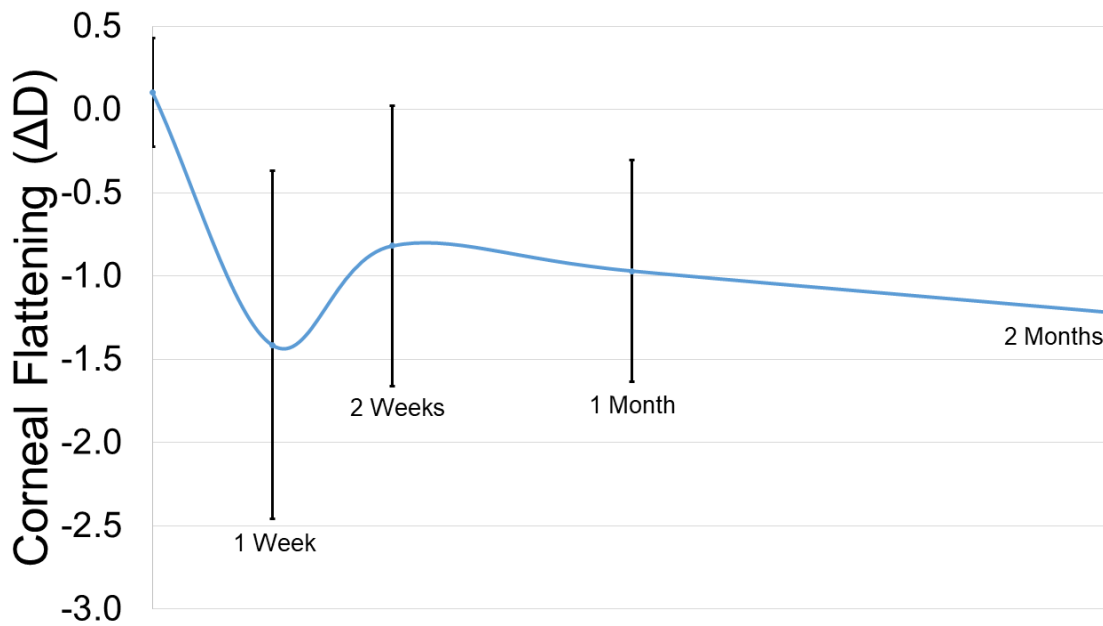


**Figure 32: Amplified NLO CXL Induced Corneal Flattening**

Graph of corneal flattening measured as change in diopter of right versus left eye over all time points. Corneal flattening decreased dramatically after one week of healing, then reverted slightly and began to flatten more steadily.

**Table 5: Corneal Flattening Data**

<b>Rabbit</b>	<b>Base</b>	<b>1 Week</b>	<b>2 Week</b>	<b>1 Month</b>	<b>2 Month</b>
<b>1</b>	-0.2	-3.0	-1.2	-0.3	-2.3
<b>2</b>	0.4	-1.7	-1.3	-1.1	-2.2
<b>3</b>	0.5	-0.5	0.1	-0.2	-1.0
<b>4</b>	-0.2	-2.6	-1.3	-0.6	-0.9
<b>5</b>	-0.2	-0.7	-0.3	-1.0	-0.3
<b>6</b>	0.4	-0.4	-2.0	-1.7	-1.0
<b>7</b>	0.0	-1.0	0.2	-1.9	-0.8
<b>Mean</b>	0.1	-1.4	-0.8	-1.0	-1.2
<b>SD</b>	0.3	1.0	0.8	0.7	0.7

## **Discussion**

Our previous method of NLO CXL using non amplified fs pulses was able to produce successful crosslinking. With that system we were able to quickly scan a crosslinked volume into corneal tissue which produced an increased corneal stiffness, and blue CAF, but the average power required to do this was more than 17 times the ANSI limit.<sup>31, 32</sup> By utilizing amplified fs pulses we were able to design a new system which produces crosslinking using a much lower average power, remaining under the ANSI limit. This study explored the effects of amplified NLO CXL in both ex vivo and in vivo models. To our knowledge it is the first report using amplified fs pulses for photodynamic therapy that does not involve optical breakdown.

During ex vivo experiments, it was discovered that the laser scanning speed is logarithmically related to the CAF intensity. A scan speed of 15.5 mm/s was found to have

comparable CAF to traditional UVA CXL. For this reason the 20mm/s was used for all other experiments. We have also shown in this study that amplified NLO CXL is still capable of producing a significant increase in mechanical stiffness of corneal tissue, 1.6 times stiffer than control.

Many other studies have explored the in vivo effects of UVA CXL and found effects on corneal structure, specifically a flattening of at least one diopter lasting a year or longer.<sup>13, 15-17, 19</sup> This has increased the interest for use of corneal crosslinking to treat low refractive errors. Like UVA CXL, NLO CXL was a treatment originally designed to re-strengthen corneas weakened by ectatic disease. This study showed that it is possible to achieve flattening with amplified NLO CXL as well, broadening the scope of this treatment to treat low refractive errors as well as corneal ectasia. Unlike UVA CXL, amplified NLO CXL has the ability to treat the cornea in a precise geometric pattern at any depth within the cornea. With this ability it could theoretically be possible to treat customize crosslinking to match an individual patient's needs, or to crosslink below an intact epithelium without damaging the epithelial cells, resulting in a more effective and less painful procedure.

One remaining question left unanswered by this study is a physical explanation of why amplified fs pulses are able to produce crosslinking equal to our previous studies which used 80 times the total deposited energy.<sup>31, 32</sup> One possible explanation involves the fluorescence lifetime of riboflavin compared to the timing of the laser pulses. The excited singlet state of riboflavin has a fluorescence lifetime of 5 ns, after which the molecule either emits a photon (fluorescence) or undergoes intersystem crossing to the excited triplet state. The triplet state is the pathway necessary for NLO CXL and has a

half-life of roughly 15  $\mu$ s. In our previous studies, the laser repetition rate was 80 MHz, or 1 pulse every 12.5 nanoseconds. Since the triplet state lifetime of riboflavin is 3 orders of magnitude longer than the time between pulses, it's likely the triplet riboflavin absorbed additional photons elevating it to the excited triplet state. From here, the molecule could either vibrationally relax to the ground triplet state and ultimately react with oxygen, or it could return to the excited singlet state via reverse intersystem crossing.<sup>62</sup> In the latter case, the riboflavin would have absorbed 4 photons without having led to any crosslinking. Furthermore, this same riboflavin molecule could potentially cross to the triplet state again, absorb a further two photons, and ultimately end up in the singlet state any number of times without having contributed to free oxygen radical generation and thus crosslinking. This could account for the tremendous loss in the total energy requirement we observed in switching from MHz pulses to amplified pulses in the kHz regime (1000 J vs. 10 J). In this chapter, the time separation between pulses was 10  $\mu$ s, thus drastically reducing the likelihood of further excitation of the triplet state. Future experiments will be needed to test this theory.

# Chapter 6: Conclusions and Future Work

## Conclusions

### *Crosslinking as a Treatment:*

#### *Keratoconus and Post LASIK Ectasia*

Crosslinking of the corneal sclera was originally intended to treat ectatic diseases which weaken the corneal collagen matrix such as Keratoconus and post LASIK ectasia. UVA CXL, the FDA approved and traditional method, has proven to be a rather effective means of delaying the progression of ectatic disease. It is able to produce an increase in stiffness of human corneas of up to 300%, with a 2-3 fold increase in elastic modulus.<sup>7, 11</sup> While this method is very simple and effective, it is also imprecise, painful, and damaging to cellular structures. As described in the whole of this text, NLO CXL is a much more precise and possibly less damaging way to achieve the same result. We have demonstrated the ability of both non-amplified and amplified fs pulses, using devices of our own design, to produce comparable effects to traditional UVA CXL, namely increased mechanical stiffness and enhanced CAF.<sup>31, 32</sup>

#### *Myopia*

Myopia is the most common refractive error and is estimated to affect 1.6 billion people worldwide, with a prevalence of 33% in the United States and up to 80-90% in East Asian young adults.<sup>63, 64</sup> Since its introduction nearly 30 years ago, laser assisted in situ keratomileusis (LASIK) has become the standard of care for surgical correction of refractive errors, including myopia, in the human eye.<sup>65</sup> The procedure entails cutting a corneal flap and ablating the stroma underneath with an excimer laser, thus modifying

corneal curvature to better focus light onto the retina. Despite high patient satisfaction rates (>95%) with LASIK,<sup>66</sup> many patients such as those with thin corneas, forme fruste, or those with mild refractive errors are not ideal candidates for the procedure. Specifically in patients with low refractive error ( $\pm 2$  diopters), the risks associated with LASIK may outweigh the benefits of a successful surgery. These patients can typically function day to day uncorrected, opting to wear glasses only during certain activities such as driving. This creates an unmet medical need for a less invasive, safer procedure for the correction of low refractive errors.

In recent years, a number of technologies have emerged with the potential to provide a safer, less invasive refractive surgery for low refractive errors. The first technology in this category, UVA CXL, which has already been talked about extensively in previous chapters, has been increasingly investigated as a refractive procedure.<sup>7, 67</sup> With respect to Keratoconus, the goal of CXL is to halt the progression of the disease by mechanically strengthening the corneal tissue. In regards to potential refractive CXL, the goal is to selectively alter the biomechanical properties of the corneal stroma via collagen crosslinks, thereby changing the topography of the cornea and correcting vision.

While UVA CXL is the most commonly used method to achieve corneal collagen crosslinking, our group has previously used the NLO CXL method already described to crosslink corneal collagen.<sup>29, 31, 32</sup> Using this technique we achieved corneal collagen crosslinking and mechanical stiffening on par with UVA CXL,<sup>31, 32</sup> indicating that NLO CXL also has the potential to correct low refractive errors. As described above, we hypothesized that amplified NLO CXL has the potential to produce the same benefits as our previous NLO CXL system, and UVA CXL, including the potential for producing

corneal flattening. Amplified NLO CXL was carried out in live rabbits and topography was measured to assess refractive outcomes of amplified NLO CXL in a live animal model, and a decrease of 1.2 Diopters was measured after 2 months.

### *Effects of Corneal Crosslinking:*

As outlined in Chapter 4, the majority of the effects of crosslinking in the corneal stroma are still greatly debated within the literature. For example, most agree that the procedure results in cellular death, corneal haze, enhanced CAF, and collagen fiber thickening, but there is debate as to which of these are related and what causes them.<sup>7, 12, 14-16, 22</sup> Our study in Chapter 4 was able to link crosslinking to a decrease in collagen fiber crimping, which we suggest could be related to the reported decrease in corneal curvature.<sup>27</sup> However, this connection is far from known. Also, many reports list varying times for cellular repopulation from 4 to 6 weeks,<sup>23-25</sup> though our result showed only peripheral repopulation as far out as 3 months.<sup>27</sup> With so little agreement on the effects of traditional UVA CXL it is hard to say how the cornea will react to NLO CXL based on that alone. Though it is thought that the increased precision of the procedure could reduce some of the more disagreeable effects, such as cellular damage.

## **Future Work**

### *Trans-epithelial Crosslinking:*

In this report we have shown that NLO CXL can be used for highly controllable crosslinking of the corneal stroma, even within ANSI power limits. What was not thoroughly explored was the impact that a drastic increase in precision could have on a

crosslinking procedure, whether it be for treatment of ectatic disease or myopia. Because of the nature of two photon excitation, the region of crosslinking can be placed anywhere within the cornea, at any depth and then scanned into any conceivable pattern that can be programmed into the software. This opens up two possibilities for NLO CXL that UVA CXL will always struggle with.

First, patients can be treated as individuals. When the day comes that mapping and modeling can show exactly what alterations will produce a desired effect in a patient's cornea, NLO CXL can make those highly variable alterations, with its micron control over placement within the tissue. Second, trans-epithelial crosslinking is a more viable option with NLO CXL. Avoiding epithelial debridement is of particular interest because this is the most painful part of the procedure. It also leads to delayed visual recovery and increases the risk of bacterial keratitis and corneal ulceration.<sup>68</sup> Many have studied trans-epithelial UVA CXL, with minimal success.<sup>14, 21</sup> The biggest reported hurdle for this is the fact that the corneal epithelium is impermeable to riboflavin. Much of the research is focused on finding the right drug or method to get riboflavin into the stroma without damaging this cell layer. Perhaps the most common method of doing so is to add the drug Benzalkonium Chloride, or BAK.

We have performed preliminary experiments on the penetration of riboflavin across the corneal endothelium and found the addition of 0.01% BAK to allow an average of 2.33 µg/ml into the stroma. This is only a fraction of the 9.5 µg/ml measured after traditional epithelial removal, Figure 33. If the riboflavin concentration is increased to 1% more than the desired amount makes it into the stroma, but it is not known what other effect this could have. Also, not only is BAK known to be harmful in large doses,<sup>69</sup> UVA irradiation

is definitely harmful. Due to the single photon excitation process of UVA CXL, there is no way to avoid generation of oxygen free radical within the epithelial layer. So, even if a perfect method of riboflavin penetration across the corneal epithelium can be found, there is no way to avoid damage from the subsequent treatment. With NLO CXL this is less of an issue, since the light can be focused below the epithelium with little or no effect to the area above.

As a proof of this concept, *ex vivo* rabbit corneas were soaked in riboflavin solution containing 0.01% BAK without removal of the epithelium and raster scanned with 0.2 NA, at 15 mm/s, and under 5 mW of average power (using the amplified pulse system detailed in the issues section of Chapter 2). Speed was chosen to avoid any overlapping of pulses on a single spot. For comparison, some eyes were also treated using trans-epithelial UVA CXL using the same BAK riboflavin solution. CAF within vibratome sections was used to compare the crosslinking between samples. Images taken within NLO CXL (34B), showed highly defined lines consistent with the scanning parameters used, demonstrating the ability of a single fs pulse to induce crosslinking below an intact epithelium at very low average power. Also, trans-epithelial UVA CXL eyes appeared to show epithelial damage. This suggests that NLO CXL using amplified fs pulses may be an effective method of precisely inducing crosslinking without damaging the epithelium.

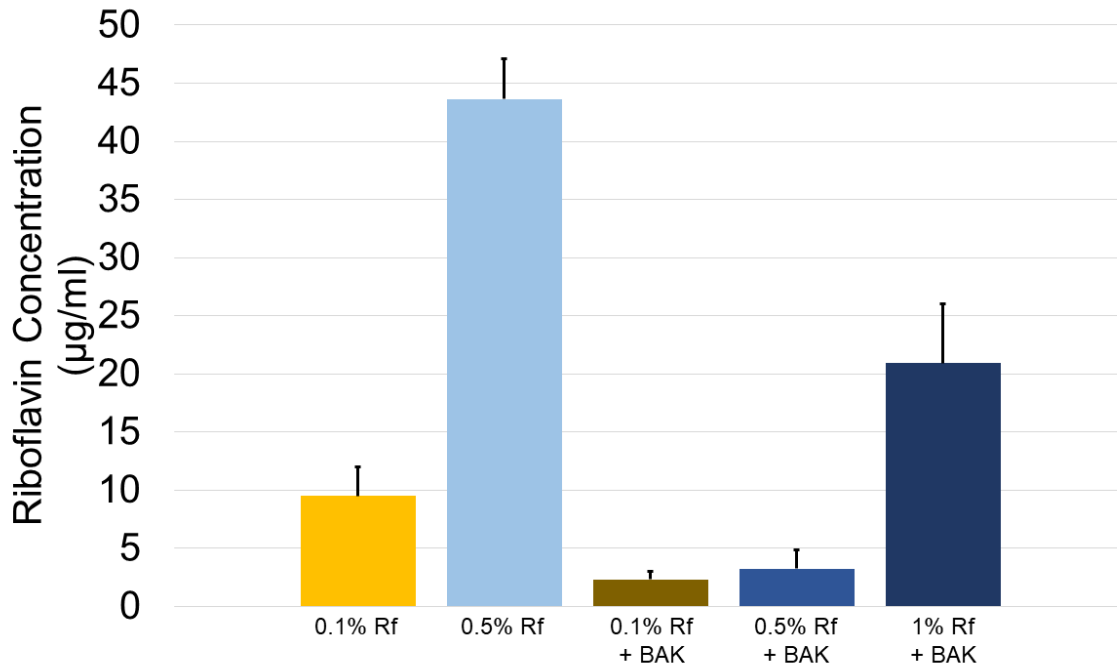


**Figure 33: Riboflavin Penetration across the Corneal Epithelium**

Shown above are the measured concentrations of riboflavin within the corneal stroma after 30 minutes of dripping in five cases, 0.1% and 0.5% riboflavin after epithelial removal, 0.1% riboflavin with 0.01% BAK and no epithelial removal, 0.5% riboflavin with BAK and no removal, and 1% riboflavin with BAK and no removal.

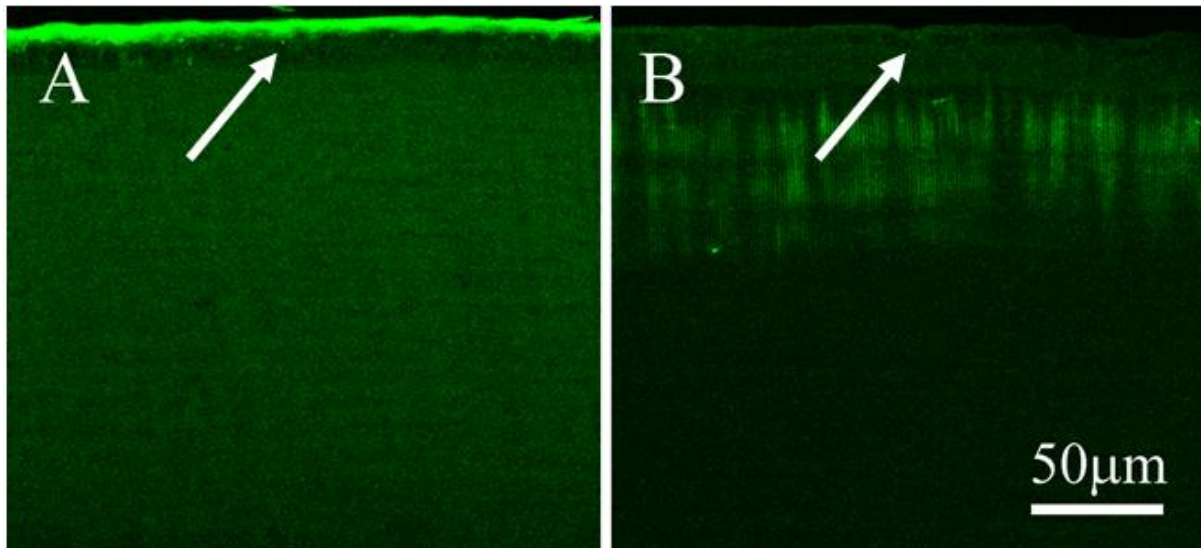


**Figure 34: Comparison of Trans-epithelial UVA and Amplified NLO CXL**

Images A and B show CAF of a representative corneal section treated with trans-epithelial UVA CXL and trans-epithelial amplified NLO CXL, respectively with arrows pointing to each epithelium. Image C shows the border between the treated area and the periphery of a trans-epithelial UVA CXL sample.

### *Further Investigation of Amplified NLO CXL:*

In addition to trans-epithelial crosslinking, future NLO CXL studies need to be devoted to further investigation of amplified pulse crosslinking. They should be devoted at least partially to exploring the behavior of amplified pulses and the relationship between pulse energy, repetition rate, and the resulting crosslinking effects. One such experiment that is already being planned will attempt to confirm the theory described in the previous chapter relating to the half-life of riboflavin pulses. We hypothesize that if that theory is true, multiple overlapping pulses spaced well beyond the half-life of the triplet state of riboflavin will result in higher CAF intensity than a single pulse or rapidly overlapped pulses. If riboflavin is allowed to relax before another pulse arrives, a greater crosslinking effect will be seen.

# Bibliography

1. Winkler M, Chai D, Kriling S, et al. Nonlinear optical macroscopic assessment of 3-D corneal collagen organization and axial biomechanics. *Investigative ophthalmology & visual science*. 2011;52:8818-8827.
2. Morishige N, Wahlert AJ, Kenney MC, et al. Second-harmonic imaging microscopy of normal human and keratoconus cornea. *Investigative ophthalmology & visual science*. 2007;48:1087-1094.
3. Vellara HR, Patel DV. Biomechanical properties of the keratoconic cornea: a review. *Clinical & experimental optometry*. 2015;98:31-38.
4. Cunningham WJ, Brookes NH, Twohill HC, et al. Trends in the distribution of donor corneal tissue and indications for corneal transplantation: the New Zealand National Eye Bank Study 2000-2009. *Clin Exp Ophthalmol*. 2012;40:141-147.
5. Randleman JB, Trattler WB, Stulting RD. Validation of the Ectasia Risk Score System for preoperative laser in situ keratomileusis screening. *American journal of ophthalmology*. 2008;145:813-818.
6. Spoerl E, Huhle M, Seiler T. Induction of cross-links in corneal tissue. *Experimental eye research*. 1998;66:Experimental eye research:97-103.
7. Wollensak G, Spoerl E, Seiler T. Riboflavin/ultraviolet-a-induced collagen crosslinking for the treatment of keratoconus. *American journal of ophthalmology*. 2003;135:American journal of ophthalmology:620-627.
8. Raiskup F, Spoerl E. Corneal crosslinking with riboflavin and ultraviolet A. I. Principles. *Ocul Surf*. 2013;11:65-74.
9. Kamaev P, Friedman MD, Sherr E, Muller D. Photochemical kinetics of corneal cross-linking with riboflavin. *Investigative ophthalmology & visual science*. 2012;53:Investigative ophthalmology & visual science:2360-2367.
10. Chai D, Gaster RN, Roizenblatt R, Juhasz T, Brown DJ, Jester JV. Quantitative assessment of UVA-riboflavin corneal cross-linking using nonlinear optical microscopy. *Investigative ophthalmology & visual science*. 2011;52:Investigative ophthalmology & visual science:4231-4238.
11. Wollensak G, Iomdina E. Long-term biomechanical properties of rabbit cornea after photodynamic collagen crosslinking. *Acta Ophthalmol*. 2009;87:48-51.
12. Malik S, Humayun S, Nayyar S, Ishaq M. Determining the efficacy of corneal crosslinking in progressive keratoconus. *Pak J Med Sci*. 2017;33:389-392.
13. Hersh PS, Stulting RD, Muller D, Durrie DS, Rajpal RK. United States Multicenter Clinical Trial of Corneal Collagen Crosslinking for Keratoconus Treatment. *Ophthalmology*. 2017.
14. Shalchi Z, Wang X, Nanavaty MA. Safety and efficacy of epithelium removal and transepithelial corneal collagen crosslinking for keratoconus. *Eye (Lond)*. 2015;29:15-29.
15. Kanellopoulos AJ, Asimellis G. Combined laser in situ keratomileusis and prophylactic high-fluence corneal collagen crosslinking for high myopia: two-year safety and efficacy. *Journal of cataract and refractive surgery*. 2015;41:1426-1433.
16. De Bernardo M, Capasso L, Lanza M, et al. Long-term results of corneal collagen crosslinking for progressive keratoconus. *J Optom*. 2015;8:180-186.
17. Elling M, Kersten-Gomez I, Dick HB. Photorefractive intrastromal corneal crosslinking for the treatment of myopic refractive errors: Six-month interim findings. *Journal of cataract and refractive surgery*. 2017;43:789-795.
18. Raiskup-Wolf F, Hoyer A, Spoerl E, Pillunat LE. Collagen crosslinking with riboflavin and ultraviolet-A light in keratoconus: long-term results. *Journal of cataract and refractive surgery*. 2008;34:796-801.

19. Vinciguerra P, Albe E, Trazza S, Seiler T, Epstein D. Intraoperative and postoperative effects of corneal collagen cross-linking on progressive keratoconus. *Archives of ophthalmology*. 2009;127:1258-1265.
20. Hagem AM, Thorsrud A, Sandvik GF, Raen M, Drolsum L. Collagen crosslinking with conventional and accelerated ultraviolet-A irradiation using riboflavin with hydroxypropyl methylcellulose. *Journal of cataract and refractive surgery*. 2017;43:511-517.
21. Lombardo G, Micali NL, Villari V, et al. Assessment of stromal riboflavin concentration-depth profile in nanotechnology-based transepithelial corneal crosslinking. *Journal of cataract and refractive surgery*. 2017;43:680-686.
22. Wollensak G, Spoerl E, Wilsch M, Seiler T. Endothelial cell damage after riboflavin-ultraviolet-A treatment in the rabbit. *Journal of cataract and refractive surgery*. 2003;29:1786-1790.
23. Kozobolis V, Gkika M, Sideroudi H, et al. Effect of Riboflavin/UVA Collagen Cross-linking on Central Cornea, Limbus and Intraocular Pressure. Experimental Study in Rabbit Eyes. *Acta Medica (Hradec Kralove)*. 2016;59:91-96.
24. Kruger A, Hovakimyan M, Ramirez Ojeda DF, et al. Combined nonlinear and femtosecond confocal laser-scanning microscopy of rabbit corneas after photochemical cross-linking. *Investigative ophthalmology & visual science*. 2011;52:4247-4255.
25. Wollensak G, Iomdina E, Dittert DD, Herbst H. Wound healing in the rabbit cornea after corneal collagen cross-linking with riboflavin and UVA. *Cornea*. 2007;26:600-605.
26. Wollensak G, Spoerl E, Wilsch M, Seiler T. Keratocyte apoptosis after corneal collagen cross-linking using riboflavin/UVA treatment. *Cornea*. 2004;23:43-49.
27. Bradford SM, Mikula ER, Juhasz T, Brown DJ, Jester JV. Collagen fiber crimping following in vivo UVA-induced corneal crosslinking. *Experimental eye research*. 2018;177:173-180.
28. Spoerl E, Mrochen M, Sliney D, Trokel S, Seiler T. Safety of UVA-riboflavin cross-linking of the cornea. *Cornea*. 2007;26:Cornea:385-389.
29. Chai D, Juhasz T, Brown DJ, Jester JV. Nonlinear optical collagen cross-linking and mechanical stiffening: a possible photodynamic therapeutic approach to treating corneal ectasia. *Journal of biomedical optics*. 2013;18:Journal of biomedical optics:038003.
30. Zipfel WR, Williams RM, Webb WW. Nonlinear magic: multiphoton microscopy in the biosciences. *Nature biotechnology*. 2003;21:Nature biotechnology:1369-1377.
31. Bradford SM, Brown DJ, Juhasz T, Mikula E, Jester JV. Nonlinear optical corneal collagen crosslinking of ex vivo rabbit eyes. *J Cataract Refract Surg*. 2016;42:1660-1665.
32. Bradford SM, Mikula ER, Chai D, Brown DJ, Juhasz T, Jester JV. Custom built nonlinear optical crosslinking (NLO CXL) device capable of producing mechanical stiffening in ex vivo rabbit corneas. *Biomed Opt Express*. 2017;8:4788-4797.
33. Cui L, Huxlin KR, Xu L, MacRae S, Knox WH. High-resolution, noninvasive, two-photon fluorescence measurement of molecular concentrations in corneal tissue. *Investigative ophthalmology & visual science*. 2011;52:2556-2564.
34. Zhang Y, Conrad AH, Conrad GW. Effects of ultraviolet-A and riboflavin on the interaction of collagen and proteoglycans during corneal cross-linking. *The Journal of biological chemistry*. 2011;286:13011-13022.
35. Levental I, Levental KR, Klein EA, et al. A simple indentation device for measuring micrometer-scale tissue stiffness. *J Phys Condens Matter*. 2010;22:194120.
36. Hayes WC, Keer LM, Herrmann G, Mockros LF. A mathematical analysis for indentation tests of articular cartilage. *Journal of biomechanics*. 1972;5:Journal of biomechanics:541-551.
37. Thomasy SM, Raghunathan VK, Winkler M, et al. Elastic modulus and collagen organization of the rabbit cornea: epithelium to endothelium. *Acta biomaterialia*. 2014;10:785-791.

38. Liu J, Roberts CJ. Influence of corneal biomechanical properties on intraocular pressure measurement: quantitative analysis. *Journal of cataract and refractive surgery*. 2005;31:146-155.
39. Delori FC, Webb RH, Sliney DH, American National Standards I. Maximum permissible exposures for ocular safety (ANSI 2000), with emphasis on ophthalmic devices. *J Opt Soc Am A Opt Image Sci Vis*. 2007;24:1250-1265.
40. Li J, Jester JV, Cavanagh HD, Black TD, Petroll WM. On-line 3-dimensional confocal imaging in vivo. *Investigative ophthalmology & visual science*. 2000;41:2945-2953.
41. Mazzotta C, Hafezi F, Kymionis G, et al. In Vivo Confocal Microscopy after Corneal Collagen Crosslinking. *Ocul Surf*. 2015;13:298-314.
42. Moller-Pedersen T, Li HF, Petroll WM, Cavanagh HD, Jester JV. Confocal microscopic characterization of wound repair after photorefractive keratectomy. *Investigative ophthalmology & visual science*. 1998;39:487-501.
43. Grytz R, Meschke G. A computational remodeling approach to predict the physiological architecture of the collagen fibril network in corneo-scleral shells. *Biomech Model Mechanobiol*. 2010;9:225-235.
44. Ho LC, Sigal IA, Jan NJ, et al. Magic angle-enhanced MRI of fibrous microstructures in sclera and cornea with and without intraocular pressure loading. *Investigative ophthalmology & visual science*. 2014;55:5662-5672.
45. Kamma-Lorger CS, Boote C, Hayes S, et al. Collagen and mature elastic fibre organisation as a function of depth in the human cornea and limbus. *J Struct Biol*. 2010;169:424-430.
46. Meek KM, Fullwood NJ. Corneal and scleral collagens--a microscopist's perspective. *Micron*. 2001;32:261-272.
47. Pierlot CM, Lee JM, Amini R, Sacks MS, Wells SM. Pregnancy-induced remodeling of collagen architecture and content in the mitral valve. *Ann Biomed Eng*. 2014;42:2058-2071.
48. Pijanka JK, Coudrillier B, Ziegler K, et al. Quantitative mapping of collagen fiber orientation in non-glaucoma and glaucoma posterior human sclerae. *Investigative ophthalmology & visual science*. 2012;53:5258-5270.
49. Han M, Giese G, Bille J. Second harmonic generation imaging of collagen fibrils in cornea and sclera. *Opt Express*. 2005;13:5791-5797.
50. Mercatelli R, Ratto F, Rossi F, et al. Three-dimensional mapping of the orientation of collagen corneal lamellae in healthy and keratoconic human corneas using SHG microscopy. *J Biophotonics*. 2017;10:75-83.
51. Park CY, Lee JK, Chuck RS. Second Harmonic Generation Imaging Analysis of Collagen Arrangement in Human Cornea. *Investigative ophthalmology & visual science*. 2015;56:5622-5629.
52. Quantock AJ, Winkler M, Parfitt GJ, et al. From nano to macro: studying the hierarchical structure of the corneal extracellular matrix. *Experimental eye research*. 2015;133:81-99.
53. Tan HY, Chang YL, Lo W, et al. Characterizing the morphologic changes in collagen crosslinked-treated corneas by Fourier transform-second harmonic generation imaging. *Journal of cataract and refractive surgery*. 2013;39:779-788.
54. Zyablitskaya M, Takaoka A, Munteanu EL, Nagasaki T, Trokel SL, Paik DC. Evaluation of Therapeutic Tissue Crosslinking (TXL) for Myopia Using Second Harmonic Generation Signal Microscopy in Rabbit Sclera. *Investigative ophthalmology & visual science*. 2017;58:21-29.
55. Doughty MJ. The cornea and corneal endothelium in the aged rabbit. *Optom Vis Sci*. 1994;71:809-818.
56. Muller LJ, Pels E, Vrensen GF. The specific architecture of the anterior stroma accounts for maintenance of corneal curvature. *Br J Ophthalmol*. 2001;85:437-443.
57. Sondergaard AP, Ivarsen A, Hjortdal J. Reduction of stromal swelling pressure after UVA-riboflavin cross-linking. *Investigative ophthalmology & visual science*. 2013;54:1625-1634.

58. Wollensak G, Wilsch M, Spoerl E, Seiler T. Collagen fiber diameter in the rabbit cornea after collagen crosslinking by riboflavin/UVA. *Cornea*. 2004;23:503-507.
59. Chai D, Gaster RN, Roizenblatt R, Juhasz T, Brown DJ, Jester JV. Quantitative assessment of UVA-riboflavin corneal cross-linking using nonlinear optical microscopy. *Invest Ophthalm Vis Sci*. 2011;52:4231.
60. Steven P, Hovakimyan M, Guthoff RF, Huttmann G, Stachs O. Imaging corneal crosslinking by autofluorescence 2-photon microscopy, second harmonic generation, and fluorescence lifetime measurements. *Journal of cataract and refractive surgery*. 2010;36:2150-2159.
61. Franco W, Ortega-Martinez A, Zhu H, Wang RS, Kochevar IE. Fluorescence spectroscopy of collagen crosslinking: non-invasive and in-situ evaluation of corneal stiffness. *Proc Spie*. 2015;9327:Proc Spie.
62. Hu DH, Yao L, Yang B, Ma YG. m Reverse intersystem crossing from upper triplet levels to excited singlet: a 'hot excitation' path for organic light-emitting diodes. *Philos T R Soc A*. 2015;373:Philos T R Soc A.
63. Wu PC, Huang HM, Yu HJ, Fang PC, Chen CT. Epidemiology of Myopia. *Asia Pac J Ophthalmol (Phila)*. 2016;5:386-393.
64. Vitale S, Ellwein L, Cotch MF, Ferris FL, 3rd, Sperduto R. Prevalence of refractive error in the United States, 1999-2004. *Archives of ophthalmology*. 2008;126:1111-1119.
65. Reinstein DZ, Archer TJ, Gobbe M. The history of LASIK. *Journal of refractive surgery*. 2012;28:291-298.
66. Solomon KD, Fernandez de Castro LE, Sandoval HP, et al. LASIK world literature review: quality of life and patient satisfaction. *Ophthalmology*. 2009;116:691-701.
67. Lim WK, Soh ZD, Choi HKY, Theng JTS. Epithelium-on photorefractive intrastromal cross-linking (PiXL) for reduction of low myopia. *Clin Ophthalmol*. 2017;11:1205-1211.
68. Perez-Santonja JJ, Artola A, Javaloy J, Alio JL, Abad JL. Microbial keratitis after corneal collagen crosslinking. *Journal of cataract and refractive surgery*. 2009;35:1138-1140.
69. Sarkar J, Chaudhary S, Namavari A, et al. Corneal neurotoxicity due to topical benzalkonium chloride. *Investigative ophthalmology & visual science*. 2012;53:1792-1802.